

# Dynamics of a Solidifying Icy Satellite Shell

Jacob Buffo<sup>1,1</sup>, C R Meyer<sup>1,1</sup>, and J R G Parkinson<sup>2,2</sup>

<sup>1</sup>Dartmouth College

<sup>2</sup>Oxford University

November 30, 2022

## Abstract

Ocean worlds have been identified as high-priority astrobiology targets due to the link between life and liquid water. Young surface terrain on many icy bodies indicates they support active geophysical cycles that may facilitate ocean-surface transport that could provide observables for upcoming missions. Accurately interpreting spacecraft observations requires constraining the relationship between ice shell characteristics and interior dynamics. On Earth, the composition, physical characteristics, and bioburden of ocean-derived ices are related to their formation history and parent fluid composition. In such systems the ice-ocean interface, which exists as a multiphase mushy layer, dictates the overlying ice's properties and evolution. Inclusion of the physics governing these boundaries is a novel strategy in modeling planetary ices, and thus far has been limited to 1D approaches. Here we present results from 2D simulations of an archetypal ice-ocean world. We track the evolution of temperature, salinity, porosity, and brine velocity within a thickening ice shell enabling us to place improved constraints on ice-ocean world properties, including: the composition of planetary ice shells, the thickness and hydraulic connectivity of ice-ocean interfaces, and heterogeneous dynamics/structures in the interfacial mushy layer. We show that stable eutectic horizons are likely a common feature of ice-ocean worlds and that ocean composition plays an important role in governing the structure and dynamics of the interface, including the formation of chemical gradient-rich regions within the mushy layer. We discuss the geophysical and astrobiological implications of our results and highlight how they can be validated by instrument specific measurements.

# Dynamics of a Solidifying Icy Satellite Shell

J. J. Buffo<sup>1</sup>, C. R. Meyer<sup>1</sup>, and J. R. G. Parkinson<sup>2</sup>

<sup>1</sup>Thayer School of Engineering, Dartmouth College, Hanover, NH 03755, USA

<sup>2</sup>Atmospheric, Oceanic and Planetary Physics, Department of Physics, Clarendon Laboratory, University of Oxford, Parks Road, Oxford OX1 3PU, UK

## Key Points:

- The ice-ocean interfaces of icy satellites likely exist as porous layers hydraulically connected to the underlying ocean.
- Interstitial brines likely exist in regions of planetary ice shells that are above their eutectic temperature.
- Thermochemical gradients in the porous basal layer of ice shells could provide a metabolic energy source for any potential organisms.

---

Corresponding author: Jacob Buffo, [jacob.j.buffo@dartmouth.edu](mailto:jacob.j.buffo@dartmouth.edu)

**Abstract**

Ocean worlds have been identified as high-priority astrobiology targets due to the link between life and liquid water. Young surface terrain on many icy bodies indicates they support active geophysical cycles that may facilitate ocean-surface transport that could provide observables for upcoming missions. Accurately interpreting spacecraft observations requires constraining the relationship between ice shell characteristics and interior dynamics. On Earth, the composition, physical characteristics, and bioburden of ocean-derived ices are related to their formation history and parent fluid composition. In such systems the ice-ocean interface, which exists as a multiphase mushy layer, dictates the overlying ice's properties and evolution. Inclusion of the physics governing these boundaries is a novel strategy in modeling planetary ices, and thus far has been limited to 1D approaches. Here we present results from 2D simulations of an archetypal ice-ocean world. We track the evolution of temperature, salinity, porosity, and brine velocity within a thickening ice shell enabling us to place improved constraints on ice-ocean world properties, including: the composition of planetary ice shells, the thickness and hydraulic connectivity of ice-ocean interfaces, and heterogeneous dynamics/structures in the interfacial mushy layer. We show that stable eutectic horizons are likely a common feature of ice-ocean worlds and that ocean composition plays an important role in governing the structure and dynamics of the interface, including the formation of chemical gradient-rich regions within the mushy layer. We discuss the geophysical and astrobiological implications of our results and highlight how they can be validated by instrument specific measurements.

**Plain Language Summary**

Our solar system houses numerous ocean worlds that have the potential to harbor life. Typically these oceans reside beneath a thick global icy shell. Accordingly, much of what we know about these bodies relies on interpreting spacecraft observations of their icy exteriors. To illuminate the interior properties and dynamics of these worlds this requires an understanding of the relationship between internal processes and external observables. In ice-ocean environments the relationship between ice and ocean properties is governed by complex dynamics occurring at the ice-ocean interface. This interface is characterized by a slushy mixture of ice and brine (a mushy layer), whose physical structure, fluid flow, and chemical dynamics determine the resultant ice properties. Very few models of planetary ices include these dynamics, and so far there only exists one-dimensional models that do. Here we present the first two-dimensional model of planetary ices which includes the physics needed to accurately simulate the ice-ocean interface. We show that ice shell composition is governed by the two-dimensional dynamics of the ice-brine mushy layer, that the thickness of this layer scales directly with ice shell thickness, and that gradient rich regions in the mushy layer could provide sheltered and chemically favorable environments for organisms.

**1 Introduction**

The icy satellites of the outer solar system are some of the most enigmatic and inspirational bodies in planetary science, in large part due to their astrobiological potential (Des Marais et al., 2008; Hendrix et al., 2019; B. E. Schmidt, 2020). Ongoing geological activity and geomorphological features indicative of persistent subsurface water reservoirs suggests that these ice-ocean worlds may house aqueous environments suitable for the formation and evolution of life (Chivers et al., 2020; Hand et al., 2009; Marion et al., 2003; C. D. Parkinson et al., 2008; Porco et al., 2006; B. E. Schmidt, 2020; B. E. Schmidt et al., 2011). One of the most promising of these bodies is Europa (Hand et al., 2009, 2007; Marion et al., 2003; B. E. Schmidt, 2020). Europa likely possesses a global subsurface ocean (~100 km thick) underlain by a silicate mantle and roofed by a dynamic ~10-30 km thick ice shell (Schubert et al., 2004). Serpentinization reactions at the benthic water-rock interface likely provide an ongoing source of reductants to the ocean, which, when coupled with

63 surface generated oxidant delivery due to ice shell overturn (e.g. (Allu Peddinti & McNa-  
 64 mara, 2015; Buffo et al., 2020; Johnson et al., 2017)), could facilitate redox disequilibrium  
 65 chemistry favorable for metabolic processes (Vance et al., 2016). Furthermore, numerous  
 66 geological features on Europa’s surface suggest recent interaction with shallow subsurface  
 67 water reservoirs (e.g. chaos (B. E. Schmidt et al., 2011; Sotin et al., 2002) and lenticulae  
 68 (Chivers et al., 2020; Manga & Michaut, 2017; Michaut & Manga, 2014)) or even direct  
 69 expression of ocean material (e.g. plumes (Jia et al., 2018; Sparks et al., 2016) and dilational  
 70 bands (Howell & Pappalardo, 2018)), providing multiple opportunities to sample/observe  
 71 underlying reservoir and/or ocean chemistry and any biosignatures that have been entrained  
 72 in the upwelling cryohydrologic system (Kargel et al., 2000; B. E. Schmidt, 2020).

73 Europa is in good company in the outer solar system, as it is becoming increasingly  
 74 apparent that oceans are a rather ubiquitous feature of icy satellites and dwarf planets  
 75 beyond the frost line (Nimmo & Pappalardo, 2016; Buffo, 2019). Ganymede and Callisto  
 76 likely house deep subsurface oceans, potentially sandwiched between layers of high pressure  
 77 ices (Khurana et al., 1998; Vance & Brown, 2013). Enceladus’ south pole likely possesses  
 78 one of the shallowest (closest to the surface) oceans in the solar system (Nimmo, 2020),  
 79 with its iconic tiger stripes ejecting potentially endogenic materials high enough above the  
 80 moon’s surface to be analyzed by the Cassini spacecraft’s Cosmic Dust Analyzer, indicating  
 81 the presence of a salty ocean in contact with the moon’s silicate interior (Porco et al.,  
 82 2006; Hansen et al., 2011; Waite et al., 2017). If geophysical processes facilitate transport  
 83 between Titan’s hydrocarbon laden surface and its putative subsurface ocean it could create  
 84 an organic rich environment favorable for prebiotic chemistry (Fortes, 2000). Observations  
 85 of active plumes and young terrain on Triton suggest it may possess a subsurface water  
 86 reservoir (McKinnon & Kirk, 2014) (although these plumes may alternatively be generated  
 87 by the solar heating of nitrogen ice (Kirk et al., 1990)), and the New Horizons flyby revealed  
 88 geomorphological features on both Pluto and Charon that indicate the existence of either  
 89 past or present interior oceans (Bierson et al., 2020; Hammond et al., 2016). Here, we  
 90 utilize Europa as a well studied archetype for ice-ocean worlds, but note that our results  
 91 are generally applicable and/or easily extendable to other ice-ocean systems.

92 A crucial component to understanding the geophysics, habitability, and biosignature  
 93 expression mechanisms of Europa is constraining the physicochemical evolution of its ice shell  
 94 (Allu Peddinti & McNamara, 2015; Hand et al., 2007; Kargel et al., 2000; B. E. Schmidt et  
 95 al., n.d.; B. E. Schmidt, 2020; Vance et al., 2016). As the barrier to and facilitator of ocean-  
 96 surface interaction, the material and transport properties of the ice shell will govern the  
 97 geomorphological evolution of Europa’s surface, the entrainment of ocean-derived impurities  
 98 in the shell, and the chemistry of the underlying ocean (Buffo et al., 2020; Vance et al.,  
 99 2016). Moreover, the ice shell will act as the primary observational medium for upcoming  
 100 spacecraft missions (e.g. Europa Clipper, JUICE) (Pappalardo et al., 2017; Grasset et  
 101 al., 2013), which makes quantifying the relationship between empirical ice shell properties  
 102 and interior processes an imperative for optimal data interpretation and synthesis (e.g.  
 103 (Kalousová et al., 2017)). However, while numerous investigations have emphasized the  
 104 importance of physicochemical heterogeneities within and the material transport capabilities  
 105 of the ice shell to both geophysical and potential astrobiological processes on Europa (e.g.  
 106 (Barr & McKinnon, 2007; Han & Showman, 2005; Johnson et al., 2017; Kargel et al., 2000;  
 107 Vance et al., 2020)) the structural and compositional details of the shell remain largely  
 108 unconstrained. It is widely believed that Europa’s ice shell is in a stagnant lid thermal  
 109 regime; suggesting the presence of a thin ( $\sim 3\text{-}5$  km), brittle, ice lithosphere overlying a  
 110 thicker ( $\sim 10\text{-}30$  km), ductile, isothermal icy mantle undergoing solid state convection (Barr  
 111 & McKinnon, 2007; McKinnon, 1999; Schubert et al., 2004). Additionally, a number of  
 112 investigations have highlighted likely trends in non-ice material distribution within Europa’s  
 113 ice shell (e.g. (Buffo et al., 2020; Kargel et al., 2000; Zolotov & Kargel, 2009)), with higher  
 114 impurity entrainment in the shallow shell (Zolotov & Kargel, 2009) and around intrusive  
 115 hydrological features within the shell (Buffo et al., 2020) and more efficient solute rejection  
 116 as the ice shell thickened and ice-ocean interfacial growth rates slowed. Nevertheless, only

117 Buffo et al. (2020) provide quantitative estimates for the compositional profile of Europa’s  
 118 shell and themselves recognize the limitations of a one-dimensional model in an inherently  
 119 multidimensional system (Buffo et al., 2021). A similar one-dimensional approach has been  
 120 implemented to investigate the composition of Triton’s ice shell by Hammond et al. (2018).

121 Multiphase reactive porous media, or ‘mushy layers’, play a fundamental and disproportio-  
 122 nate role in the dynamics and evolution of both biogeochemical and geophysical systems  
 123 (e.g. (Loose et al., 2011; Steefel et al., 2005; Tedesco & Vichi, 2014)). The ice-ocean  
 124 layers of icy worlds, including Earth, are no exception. The complex reactive transport  
 125 processes occurring near ice-ocean interfaces govern heat and mass transport between the  
 126 two reservoirs and dictate the physicochemical properties of and impurity entrainment in  
 127 the overlying ice (Buffo et al., 2020; Hunke et al., 2011; Thomas & Dieckmann, 2008). With  
 128 direct implications for ice rheology (Assur, 1958; Durham et al., 2005), buoyancy (Han &  
 129 Showman, 2005), eutectic point (McCarthy et al., 2011, 2007), bioburden (Santibáñez et al.,  
 130 2019; Buffo, 2019; Brown et al., 2020), and conductivity (Kalousová et al., 2017) constrain-  
 131 ing the dynamics of ice-ocean/brine interfaces can improve our fundamental understanding  
 132 of icy world geophysics and aid in spacecraft data analysis/interpretation (e.g. ice penetrat-  
 133 ing radar (Schroeder et al., 2016)). Furthermore, the ice-ocean interface of terrestrial ices  
 134 provides a gradient rich substrate where both micro- and macro-fauna thrive in appreciable  
 135 densities (Ackley & Sullivan, 1994; Daly et al., 2013; Spindler, 1994; Thomas & Dieckmann,  
 136 2003).

137 It has been suggested that the thick ice shells of low-gravity moons will support thicker  
 138 multiphase boundary layers at their ice-ocean interfaces (on the order of meters to tens of  
 139 meters), as this layer’s thickness is inversely proportional to the interfacial thermal gradient  
 140 (Buffo et al., 2021). This is supported by observations of columnar sea ice formed beneath  
 141 the Ross Ice Shelf, which exhibited brine channels, high impurity entrainment, and hydraulic  
 142 connectivity to the underlying ocean throughout the bottom 6 m of ice (Zotikov et al.,  
 143 1980). Convective overturn of high salinity brine in these porous boundary layers leads to  
 144 the formation of heterogenous channel structures within the ice matrix (Cottier et al., 1999;  
 145 Wells et al., 2011; Wettlaufer et al., 1997) and can produce brinicles that extend into the  
 146 underlying ocean from the basal ice surface (Cartwright et al., 2013). As cold, saline brine  
 147 is convected out of the mushy layer in localized downwelling plumes it acts as a heat sink  
 148 for the surrounding seawater, in some cases depressing the local temperature enough that  
 149 an ice membrane forms around the saline fluid (e.g. (Mahadevan, 2017)). These tubular ice  
 150 membranes produce regions with exceptionally high thermal and chemical gradients that  
 151 could serve as an oasis for biology, akin to terrestrial hydrothermal and chemical garden  
 152 systems (Cartwright et al., 2013; Vance et al., 2019). This possibility is strengthened by the  
 153 fact that the ice-ocean interface will be the site of oxidant delivery to the ocean, providing  
 154 a redox boon for any potential organisms (Allu Peddinti & McNamara, 2015; Vance et al.,  
 155 2016).

156 Understanding the structure and dynamics of the ice-ocean interface of icy worlds has  
 157 both geophysical and astrobiological implications (Buffo et al., 2021, 2020). It is a manda-  
 158 tory port of call for ocean-surface interaction, a core-mantle boundary in the cryospheric  
 159 system that could facilitate regional geomorphological heterogeneities, and likely one of the  
 160 most habitable environments on high priority astrobiology targets. Here, we simulate the  
 161 multiphase two-dimensional evolution of Europa’s ice-ocean interface. We provide improved  
 162 constraints on the compositional profile of the growing ice shell and the relationship be-  
 163 tween ice-ocean interface thermal gradient and impurity entrainment. We show that the  
 164 multiphase ice-ocean boundary layer thickens as Europa’s ice shell thickens and interfacial  
 165 thermal gradients decrease. Additionally, we show that brinicles are a likely byproduct of  
 166 the convective overturn of brine in the porous basal ice layer. Finally, we discuss how our  
 167 estimations of ice shell structure and composition can be utilized to improve geophysical  
 168 models, constrain the habitability, and aid in spacecraft mission planning and data analysis  
 169 of Europa and other icy worlds.

## 2 Methods

To simulate the two-dimensional evolution of Europa’s ice-ocean interface we use the reactive porous media model SOFTBALL: SOLidification, Flow, and Thermodynamics in Binary ALLoys. First introduced in J. R. G. Parkinson, Martin, Wells, and Katz (2020), SOFTBALL is an open source code capable of efficiently simulating the phase evolution, heat transport, and mass transport in mushy layers. The code has been tested extensively (cf. (J. R. G. Parkinson, 2019; J. R. G. Parkinson, Martin, Wells, & Katz, 2020; Wells et al., 2019)), and we provide an additional validation of the model’s ability to reproduce the compositional and structural properties of terrestrial sea ice in Supplementary Section S1.

The equations governing the evolution of ice-ocean interfaces are well documented in the literature (e.g. (Feltham et al., 2006; Hunke et al., 2011; Worster, 1997)). Employing the Boussinesq approximation and assuming no phase change driven flow ( $\rho_{br}=\rho_i$ , where  $\rho_{br}$  is brine density, and  $\rho_i$  is ice density), conservation of mass in a reactive porous media requires

$$\nabla \cdot \mathbf{q} = 0 \quad (1)$$

where  $\mathbf{q} = (u, v)$  is the two-dimensional Darcy velocity. We assume the ice matrix is rigid and immobile and restrict mass transport to the fluid phase. Fluid flow is governed by the incompressible form of Darcy’s law

$$\mathbf{q} = -\frac{\Pi}{\mu} (\nabla p + \rho_{br} \mathbf{g}) \quad (2)$$

where  $\Pi$  is permeability (typically a function of porosity, here we utilize the Kozeny-Carman relationship given in J. R. G. Parkinson, Martin, Wells, and Katz (2020), see Eq. 7 below),  $\mu$  is the dynamic viscosity of the brine,  $p$  is dynamic pressure, and  $\mathbf{g}$  is gravity. Conservation of energy is given by

$$\frac{\partial T}{\partial t} = -\rho_{br} c_{br} \mathbf{q} \cdot \nabla T + \nabla \cdot (\bar{k} \nabla T) - \rho_i L \frac{\partial \phi}{\partial t} \quad (3)$$

where  $c$  is specific heat,  $T$  is temperature,  $k$  is thermal conductivity, and  $L$  is the latent heat of the water-ice phase transition. Quantities with overbars are volume averaged quantities (i.e.  $\bar{k} = \phi k_{br} + (1 - \phi) k_i$ , where  $\phi$  is liquid fraction (porosity)). This equation accounts for heat transport via advection and diffusion as well as the generation/usage of heat due to freezing/melting. Similarly, the conservation of salt is given by

$$\phi \frac{\partial C}{\partial t} = -\mathbf{q} \cdot \nabla C + \nabla \cdot (D \nabla C) - C \frac{\partial \phi}{\partial t} \quad (4)$$

where  $C$  is brine concentration, and  $D$  is the diffusion coefficient of the solute. We assume no salt is present in the ice phase, in line with contemporary approaches (Feltham et al., 2006; J. R. G. Parkinson, Martin, Wells, & Katz, 2020). This allows for evolution of the brine phase via advection, molecular diffusion, and concentration/dilution caused by freezing/melting of ice. The system of Equations 1-4 can be closed by assuming that the system obeys an idealised eutectic phase diagram (Figure 1a), which relates brine concentration to temperature and liquid fraction. We follow the methodology of (J. R. G. Parkinson, Martin, Wells, & Katz, 2020) (their Section 2.2 and Appendix A), and define the liquidus and solidus curves by

$$T_L(C) = T_m - mC \quad (5)$$

$$T_{Sol}(C) = T_m - mC_e \quad (6)$$

196 where  $T_L$  is the liquidus temperature,  $T_m$  is the freezing temperature of pure water,  $m$  is a  
 197 solutal freezing point depression coefficient with units of  $\text{K kg g}^{-1}$  (equivalently,  $\text{K ppt}^{-1}$ ),  
 198  $T_{Sol}$  is the solidus temperature, and  $C_e$  is the eutectic composition. If the temperature  
 199 is above the liquidus the system will be a fluid ( $\phi = 1$ ), if it is below the solidus the  
 200 system will be a solid ( $\phi = 0$ ) and any residual salt is assumed to exist as a hydrated solid  
 201 phase. Between these curves the system will exist as a mixture of pure ice and brine with  
 202 a concentration governed by Equation 5.

203 Here we simulate the top-down solidification of a hypothetical European ocean using the  
 204 initial and boundary conditions presented in Figure 1b and the physical parameter values  
 205 given in Table 1. We have chosen to use an ocean with a salinity of 35 ppt and linear liquidus  
 206 slope of  $-0.048 \text{ K/ppt}$  as this lies comfortably within the range of predicted European ocean  
 207 concentrations (Hand & Chyba, 2007; Zolotov & Shock, 2001) and compositions (Trumbo  
 208 et al., 2019; Zolotov & Shock, 2001). Simulations are initiated as a completely fluid filled  
 209 domain subject to an undercooled upper boundary ( $T_s=100 \text{ K}$ ) which induces the formation  
 210 of an ice shell. Throughout the simulation SOFTBALL tracks the evolving temperature  
 211 ( $T$ ), bulk salinity ( $C$ ), porosity ( $\phi$ ), and velocity ( $u, v$ ) within the system. By assuming  
 212 the domain exists as a thin Hele-Shaw cell a finite fluid permeability (J. R. G. Parkinson,  
 213 Martin, Wells, & Katz, 2020)

$$\Pi(\phi) = \left\{ \frac{12}{d^2} + \left[ \frac{K_0 \phi^3}{(1-\phi)^2} \right]^{-1} \right\}^{-1} \quad (7)$$

214 allows us to solve for flow throughout the entire domain using Darcy's law (Eq. 2).  $K_0$   
 215 is a permeability factor and  $d$  is the Hele-Shaw cell spacing. While an important factor in  
 216 governing the dynamic evolution of ice-brine mushy layers (Buffo et al., 2021, 2020), as it  
 217 dictates the advection of heat and solutes throughout the system, the precise permeability-  
 218 porosity relationship of ocean-derived ices remains under constrained and an active topic  
 219 of research in both terrestrial and planetary ice science (Golden et al., 2007; McCarthy et  
 220 al., 2013, 2007). Our selected permeability-porosity relationship is consistent with previous  
 221 studies of ice-ocean mushy layer systems (e.g. (Katz & Worster, 2008; J. R. G. Parkinson,  
 222 Martin, Wells, & Katz, 2020)) and agrees well with power law permeability-porosity rela-  
 223 tionships ( $\Pi(\phi) \propto \phi^n$ , where  $n \in [1, 3]$ ) that have been adopted by other studies of ice shell  
 224 mushy layers (e.g. (Buffo et al., 2020; Hammond et al., 2018)) for porosities representative of  
 225 mushy layer interiors ( $\phi < 0.8$ , see Figure 4 of Katz and Worster (2008) and Supplementary  
 226 Figure S4). The value of the permeability factor implemented here,  $K_0 = 2 \times 10^{-9} \text{ m}^2$ , was  
 227 selected such that it reproduces bulk salinity values and trends observed in terrestrial sea  
 228 ice (see Supplementary Section S1 and Supplementary Figure S3). Moreover, this value is  
 229 in agreement with reference permeabilities used in previous studies (e.g.  $K_{ref} = 10^{-9} \text{ m}^2$  in  
 230 Hammond et al. (2018) and Golden et al. (2007)). Nevertheless, both permeability-porosity  
 231 relationships and potential percolation thresholds - the limitation of fluid flow below a crit-  
 232 ical porosity (Golden et al., 2007) - have substantial implications for the dynamics and  
 233 evolution of mushy layers (Buffo et al., 2021, 2020) and constraining their values will be  
 234 essential for improving the accuracy of planetary ice shell models.

235 The Hele-Shaw cell approach optimizes computation speed as the Darcy equation is  
 236 simpler to solve than the full Navier-Stokes (a noted challenge for mushy layer systems  
 237 (Chung & Worster, 2002)) and restricting flow in the underlying fluid permits the use of  
 238 larger CFL-limited time steps. Additionally, it limits phase boundary effects (removing the  
 239 need to define interfacial conditions between the fluid and porous regions, e.g. multiple  
 240 domain Stokes-Darcy approaches (Le Bars & Worster, 2006)) while ensuring the underlying  
 241 fluid has an amplified permeability such that downwelling plumes will not stagnate and

242 artificially impact the evolution of the overlying porous region (Supplementary Section S4).  
 243 Previous works have implemented this approach to simulating mushy layers (e.g. (Wells  
 244 et al., 2019; Katz & Worster, 2008)). It should be noted that the numerical solutions in  
 245 the underlying fluid are inherently less realistic than those in the mushy layer due to the  
 246 implementation of a finite permeability. As such, results of structural and dynamic evolution  
 247 in the free fluid region should be interpreted with this in mind. We discuss the limitations  
 248 of the Hele-Shaw cell approach in describing the dynamics of the underlying fluid at length  
 249 in Supplementary Section S4.

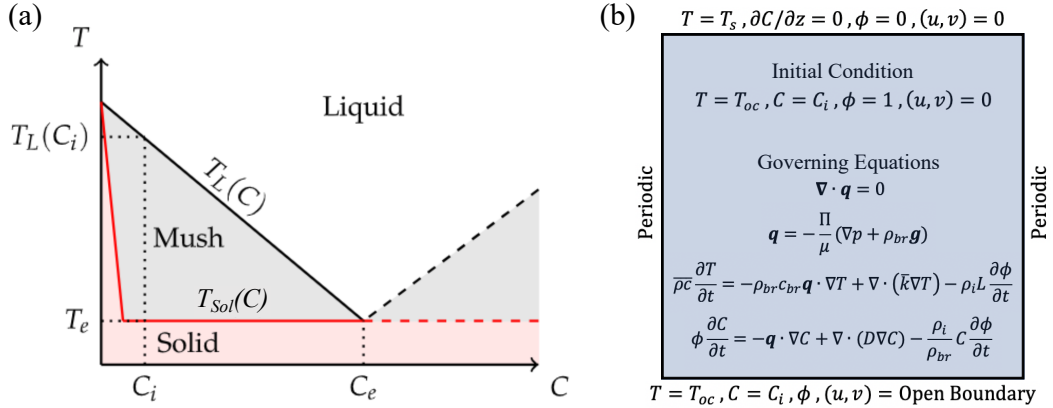


**Figure 1.** (a) – Idealized eutectic phase diagram for the ice-brine system. Above the liquidus,  $T_L(C)$ , the system exists as a pure fluid. Below the solidus,  $T_{Sol}(C)$ , the system is composed of solid ice and solid salts. Between these regions the system exists as a two-phase mush of solid ice and concentrated brine. (b) – Initial and boundary conditions utilized in the top-down solidification simulations.

### 3 Results

#### 3.1 Bulk Salinity of Europa’s Ice Shell and its Relation to Thermal Gradient

250  
 251  
 252 To constrain the bulk salinity of Europa’s ice shell we simulated the top-down solidifi-  
 253 cation of the shallow shell (0-1.1 km) using twelve different domain sizes (ranging from 10  
 254 m x 10 m to 2 km x 250 m) and resolutions (ranging from 3.9 cm to 7.8 m). The consistency  
 255 of results across a range of resolutions further validates the model’s ability to accurately  
 256 capture the continuum mechanics that govern the system, even in simulations where small  
 257 scale heterogeneities such as brine channels are not explicitly resolved. An example of the  
 258 two-dimensional bulk salinity and porosity profiles produced by such a run can be seen in  
 259 Figure 2. This particular simulation was conducted using a 20 m by 20 m domain at a  
 260 resolution of 3.9 cm (resolution results from a 512 x 512 grid) and covers the uppermost  
 261 portion of the ice shell (0-20 m). Both fossilized and active high salinity regions can be seen  
 262 throughout the thickness of the forming ice shell, suggesting a heterogeneous and apprecia-  
 263 ble distribution of salt within the ice. It is important to note that there may be additional  
 264 substructure within these regions not captured at the current simulation resolution (brine  
 265 channels in natural sea ice on Earth are typically  $\sim 1$ -3 mm in diameter), however the den-

Variable	Definition	Value
$\beta$	Density coefficient for salt	5.836e-4 kg ppt <sup>-1</sup>
$c$	Specific heat of the ocean	3985 J kg <sup>-1</sup> K <sup>-1</sup>
$c_{br}$	Specific heat of ice	2000 J kg <sup>-1</sup> K <sup>-1</sup>
$C_e$	Eutectic composition	230 ppt
$C_i$	Ocean composition	35 ppt
$d$	Hele-Shaw cell spacing	5e-5 m
$\eta$	Dynamic viscosity	1.88e-3 Pa s
$g$	Gravity	1.32 m s <sup>-2</sup>
$H$	Scale height	(varies) m
$k_{br}$	Thermal conductivity of the ocean	0.6 W m <sup>-1</sup> K <sup>-1</sup>
$k_i$	Thermal conductivity of ice	2.0 W m <sup>-1</sup> K <sup>-1</sup>
$k_s$	Salt diffusivity in water	2e-9 m <sup>2</sup> s <sup>-1</sup>
$K_0$	Permeability factor	2e-9 m <sup>2</sup>
$L$	Latent heat of fusion	334774 J kg <sup>-1</sup>
$m$	Linear liquidus slope	0.048 K ppt <sup>-1</sup>
$\phi_s$	Surface porosity	0
$\phi_{oc}$	Ocean porosity	1
$p_s$	Partition coefficient	0.001
$\rho_{br}$	Brine density	1000+1000 $\times\beta\times C$ kg m <sup>-3</sup>
$\rho_i$	Ice density	917 kg m <sup>-3</sup>
$T_e$	Eutectic temperature	273.15 - $m\times C_e$ K
$T_{oc}$	Ocean temperature	273.15 - $m\times C_i$ + 0.01 K
$T_s$	Surface temperature	100 K

**Table 1.** Variables used by the SOFTBALL code. The scale height,  $H$ , is used to define the simulation domain size and nondimensionalize the system.

266 dritic structure and density distribution (channel collapse as the ice thickens) of the high  
267 salinity regions matches both observations and theoretical predictions of ice-ocean systems  
268 (Rees Jones & Worster, 2013; Wells et al., 2011, 2019; Worster & Rees Jones, 2015; Mid-  
269 dleton et al., 2015). Also apparent is the existence of a thin (in relation to the overall  
270 ice thickness), dynamic mushy layer at the ice-ocean interface. The convective overturn of  
271 brine within this layer (Figure 2b) is responsible for the desalination of, and thus the level  
272 of ocean-derived material entrainment in, the ice shell (Buffo et al., 2020; Wells et al., 2019;  
273 Wettlaufer et al., 1997; Worster, 1997). Darcy velocities within the mushy layer range from  
274  $\sim 10^{-11}$  m/s near the ice-mush interface where porosity approaches zero and  $\sim 10^{-6}$  m/s  
275 in the downwelling saline plumes.

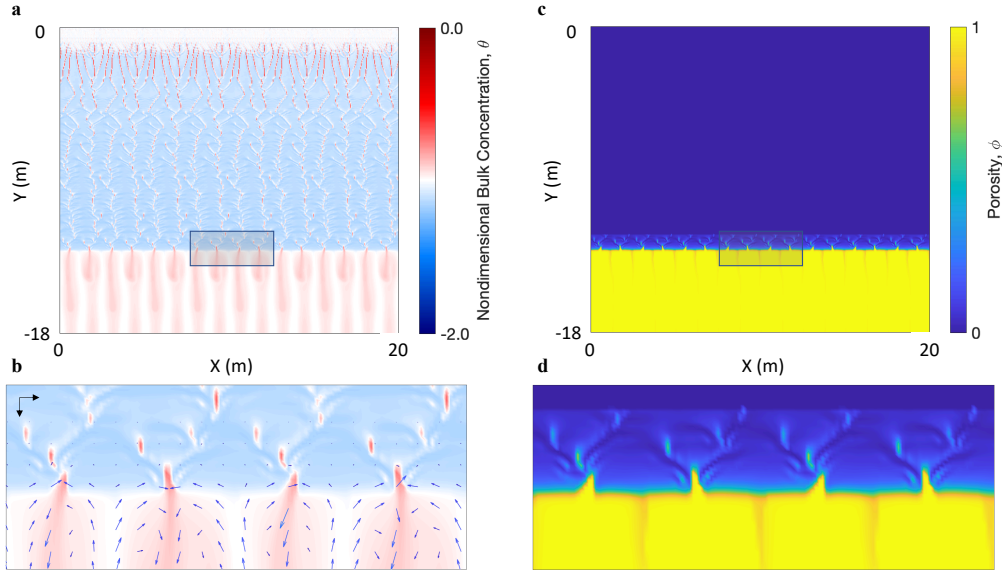


**Figure 2.** The compositional (bulk salinity) and structural (porosity) profile in Europa’s growing ice shell. **a)** Two-dimensional nondimensionalized bulk salinity profile using a scale height,  $H$ , of 10 m (domain size: 18m x 20m). Where nondimensional bulk salinity,  $\theta = \frac{C-C_e}{C_e-C_i}$ . Fossilized high salinity regions can be seen in the upper ice and dense, high salinity plumes can be seen emanating from the ice-ocean interface. **b)** Magnified view of the shaded box in panel (a), with velocity vectors included, showing the convective overturn of brine within the interfacial mushy layer. For scale, black arrows in the top left have lengths that represent Darcy velocities of  $10^{-6}$  m/s **c)** Two-dimensional porosity profile for the same region depicted in panel (a). **d)** Magnified view of the shaded box in panel (c). Low porosity brine channels are associated with high salinity downwellings.

To investigate how the ice shell composition varies with depth we horizontally average the bulk salinity of each two-dimensional run and plot it against it’s corresponding location within the shell (Figure 3a-c). It can be shown that the temperature profile in the forming ice varies negligibly from a simple conductive (linear) profile (See Supplementary Section S2), and thus the ice-ocean interface thermal gradient is well represented by

$$\frac{\partial T}{\partial z} = \frac{T_{oc} - T_s}{H_{shell}}, \quad (8)$$

where  $T_{oc}$  is ocean temperature,  $T_s$  is surface temperature, and  $H_{shell}$  is the depth of the ice-ocean interface from the surface. Plots of bulk salinity as a function of interfacial

thermal gradient can be found in Figure 3d-f. The functional form of the best fit lines closely follow the analytical solutions derived by Buffo et al. (2020) (Equations 26 & 27 of their manuscript) for the compositional evolution of a simplified ice-ocean system. Here we implement a Levenberg-Marquardt algorithm to relate bulk salinity and depth within the ice shell using the equation

$$C(z) = a + \frac{b}{c-z} [1 - d \exp(-fz)] \quad (9)$$

where  $C$  is bulk salinity,  $z$  is depth within the shell, and  $a$ ,  $b$ ,  $c$ ,  $d$ , and  $f$  are constant coefficients that account for stretches and translations. Similarly, we relate bulk salinity to thermal gradient using the equation

$$C\left(\frac{\partial T}{\partial z}\right) = a + \frac{b\left(\frac{\partial T}{\partial z} + c\right)}{\left(d + f\frac{\partial T}{\partial z}\right)} \left[1 - h \exp\left(\frac{-j}{\frac{\partial T}{\partial z}}\right)\right], \quad (10)$$

where  $a$ ,  $b$ ,  $c$ ,  $d$ ,  $f$ ,  $h$ , and  $j$  are constant coefficients that account for stretches and translations.

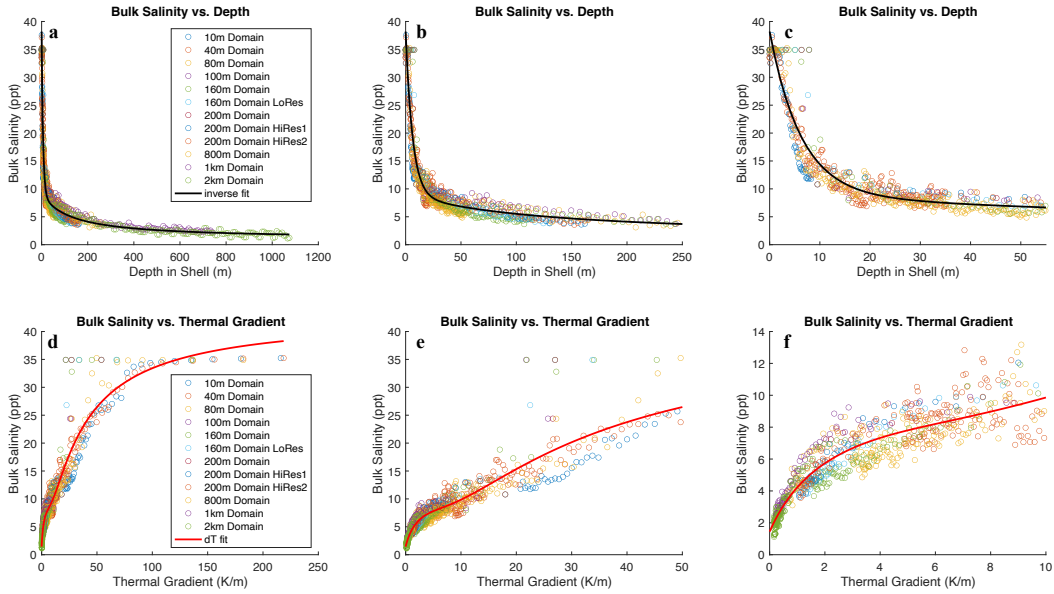


**Figure 3.** Bulk salinity characteristics of Europa’s ice shell for a 35 ppt ocean. **a-c)** Bulk salinity variation with depth in the shell. High salinity values near the surface quickly decrease with depth and asymptotically approach a lower limit of 0.984 ppt, according to the best fit line of Equation 9 (coefficients:  $a=0.984$ ,  $b=-1014$ ,  $c=-123.4$ ,  $d=-3.529$ ,  $f=0.1529$ ). **d-f)** Bulk salinity variation with ice-ocean interface thermal gradient (assuming a conductive profile in the overlying ice shell). At large thermal gradients ( $>100$  K/m) all salt is trapped within the ice. There is a prominent ‘shoulder’ region between 3-10 K/m that is captured well by the fit line of Equation 10 (coefficients:  $a=7.864$ ,  $b=-2576$ ,  $c=-5.148$ ,  $d=-2067$ ,  $f=-869.2$ ,  $h=-10.9$ ,  $j=27.2$ ). This regime could be indicative of a transition between dominant desalination mechanisms in the mushy layer (Buffo et al., 2020, 2021). (Note: Two data points with bulk salinity  $>35$  ppt visible in panels (a-c) do not appear in panels (d-f) as they are the result of interfacial thermal gradients which exceed 250 K/m. These results negligibly affect the fit lines of Equations 9 and 10 while highlighting the difficulty of accurately simulating extreme thermal environments, as we expect these values to be 35 ppt)

278 The simulated bulk salinity values are well approximated by the functional forms of  
 279 Equation 9 & 10, and exhibit a number of important trends and features predicted by earlier  
 280 studies (e.g. (Buffo et al., 2020)). These include a trend toward compositional homogeneity  
 281 as the ice shell thickens and interfacial thermal gradients decrease; a nonzero lower limit  
 282 for entrainment rate (0.98 ppt as  $z \rightarrow \infty$  and 1.45 ppt as  $\partial T/\partial z \rightarrow 0$ ), as predicted by  
 283 Equations 9 & 10, respectively); one hundred percent salt retention when ice forms under  
 284 large thermal gradients (representative of rapid freezing); and the existence of transitional  
 285 regimes in mushy layer dynamics (evidenced by the ‘shoulder’ region of Figure 3e). These  
 286 properties and their implications for the geophysics and astrobiology of Europa and other  
 287 ice-ocean worlds are discussed in Section 4.

### 288 3.2 Ice-Ocean Interface Mushy Layer Thickness

289 The porous region near the ice-ocean interface (e.g. Figure 2d) plays an important role  
 290 in governing the properties and evolution of the ice shell. This dynamic region dictates the  
 291 chemical composition and physical structure of forming ice, governs heat and solute trans-  
 292 port between the ocean and ice shell reservoirs, and determines the hydraulic connectivity  
 293 of the deep ice shell. Studies suggest that the properties of this layer are dynamic and evolve  
 294 as the overlying ice cover thickens and interfacial thermal gradients decrease (e.g. (Buffo et  
 295 al., 2021)). Furthermore, the environmental parameters (e.g. gravity, ocean composition) of  
 296 a given system will impact the layer’s structure, suggesting that a diverse array of deep ice  
 297 shell environments exist across the solar system and throughout individual ice-ocean world’s  
 298 lifetimes.

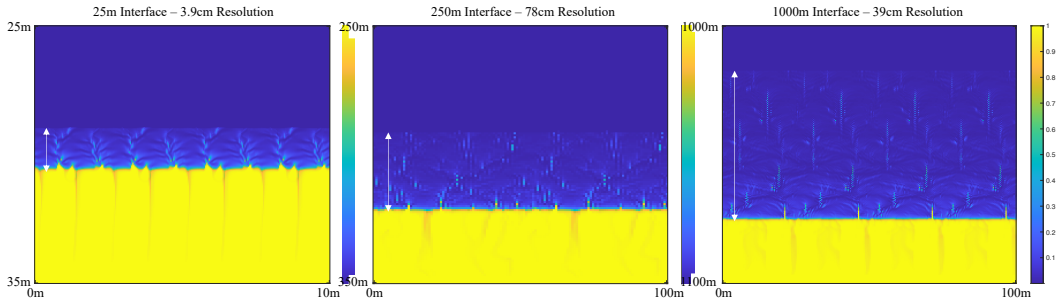


**Figure 4.** Thickness and structure of the ice-ocean interface mushy layer at various depths within the ice shell. The mushy layer thickness increases as the ice shell thickens, consistent with previous observations and theory (Buffo et al., 2021; Wells et al., 2011). The majority of fluid motion is concentrated in a high porosity region near the base of the mushy layer (e.g. Figure 2b), resulting in a ‘stagnant’ region with decreased fluid flow underlain by a thin convecting boundary layer. This was predicted theoretically by Worster (1991) for systems with large mush Rayleigh numbers, which is the case for the mushy layers considered here (see Supplementary Section S3). White arrows demarcate the horizontally averaged mushy layer thickness. (Note: The left image depicts a 10 m x 10 m domain while the center and right images depict a 100 m x 100 m domain.)

299 To constrain the evolving thickness of Europa’s ice-ocean interface mushy layer we  
 300 slightly modified the boundary conditions presented in Figure 1 such that the upper thermal  
 301 boundary was governed by a Neumann (gradient/flux) boundary condition ( $\partial T/\partial z =$   
 302  $(T_{oc} - T_s)/H_{shell}$ ) and carried out high resolution, top-down solidification simulations for  
 303 descending depths within the shell ( $H_{shell} = 0$  m, 25 m, 50 m, 100 m, 250 m, 500 m, and  
 304 1000 m). Porosity profiles during three of these runs can be seen in Figure 4. Periodically

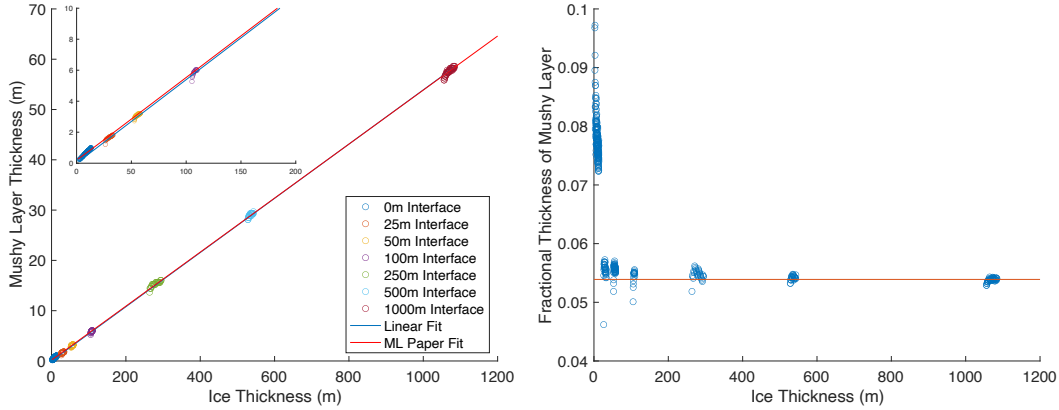


**Figure 5.** Ice-ocean interface mushy layer thickness and its relationship to ice shell thickness. **(Left)** Mushy layer thicknesses recorded during seven simulations, each initiated with a different ice-ocean interface position (overlying ice shell thickness,  $H_{shell}$ ). The relationship between mushy layer thickness and ice shell thickness is well captured by the fit line of Equation 11, here ‘ML Paper Fit’. A simple linear relationship also closely matches the data, evidenced by its overlap with the fit line of Equation 11 until the plot is magnified. (‘ML Paper Fit’ coefficients:  $a=0.02685$ ,  $b=-11.64$ ,  $c=-62.28$ ; linear relationship= $0.0539$ ). Inset – magnified view of the shallow ice shell region (0-200 m). **(Right)** The fractional percentage of the ice shell occupied by the mushy layer. The red line corresponds to the linear fit trend of 0.0539.

305 during these runs the porosity profile was horizontally averaged and the region satisfied by  
 306  $1e-5 < \phi < 0.95$  was measured, giving the mushy layer thickness. These bounds were se-  
 307 lected in lieu of  $0 < \phi < 1$  to avoid measuring any residual low porosity regions in the upper  
 308 ice shell and any high porosity structures extending from the ice-ocean interface (e.g. brin-  
 309 cles - the focus of Section 3.3). The relationship between ice-ocean interface mushy layer  
 310 thickness and ice shell thickness can be seen in Figure 5a. Figure 5b shows the fraction of  
 311 the ice shell occupied by the mushy layer and its relationship to ice shell thickness. The  
 312 increase in mushy layer thickness with growing ice shell thickness is well fit by the analytical  
 313 solution derived by (Buffo et al., 2021), (modified from Equation 25 of (Buffo et al., 2021)):

$$h_{ML} = aH_{shell} \left( 1 + \sqrt{1 - \frac{b}{H_{shell}} - \frac{c}{H_{shell}^2}} \right) \quad (11)$$

314 where  $h_{ML}$  is mushy layer thickness,  $H_{shell}$  is ice shell thickness, and  $a$ ,  $b$ , and  $c$  are constants  
 315 that allow for translations and stretches. The relationship between mushy layer thickness  
 316 and ice shell thickness is also well approximated by a simple linear trend (relationship  
 317 coefficient = 0.0539). This suggests that accretionary regions of Europa’s ice shell likely  
 318 possess a substantial multiphase ice-ocean boundary layer that occupies as much as 5%  
 319 of the ice shell thickness. Notably, the linear relationship coefficient closely matches the  
 320 eutectic horizon predicted by assuming a conductive (linear) thermal profile within the ice  
 321 shell ( $h_{eut} = \frac{T_{oc} - T_e}{T_{oc} - T_s} = 0.0548$ ). While slightly overestimating the mushy layer’s thickness,  
 322 eutectic horizons likely provide an exceptional first order estimate of ice shell hydrological  
 323 structure. This has important implications for regional and global geophysical processes,  
 324 ocean-derived material entrainment in the shell, and Europa’s potential habitability (further  
 325 discussed in Section 4).

### 3.3 Fine Scale Heterogeneities and Brinicle Formation

The fine scale structure in the multiphase region near the ice-ocean interface (e.g. Figure 2) supports thermochemical gradients that when combined with the porous nature of the ice-brine matrix could provide an ample substrate for any potential organisms. Vance et al. (2019) suggested that brinicles (hollow tubes of ice formed around downwelling brine plumes) could form at the ice-ocean interfaces of icy worlds and result in chemical garden like structures. Similar to the hydrothermally formed chemical garden systems at Earth’s seafloor, an oasis for life (Barge et al., 2015; Cartwright et al., 2002), brinicles and the mushy layer they grow from could provide a gradient rich habitat for an inverted benthic community (Cartwright et al., 2013).

To investigate the physicochemical properties of brinicles on Europa we performed high resolution simulations of the ice-ocean interface for a number of overlying ice shell thicknesses (similar to Section 3.2). The resulting porosity, brine salinity, and salinity gradient profiles for three such simulations are depicted in Figure 6. Brinicle structures can be seen extending from the mushy layer in all three cases (left column of Figure 6). The size of the brinicle structures increases with ice shell thickness. This is consistent with the convective patterns in a thickening mushy layer, where downwellings drain an increasingly large region of the mushy layer as brine channel spacing increases. Brinicle size may also be affected by their longevity. The ice-ocean interface is quite dynamic and brinicle structures grow and disappear repeatedly during simulations. The timescale over which this cycling occurs increases with depth, suggesting a thicker ice shell may promote the formation of larger and more stable ‘brinicle gardens’. The lifetimes of brinicles at an ice-ocean interface depth of 10 m, 50 m, and 1000 m are on the order of hours, days, and years, respectively. Salinity gradients are highest near brine channels within the mushy layer and at the edges of downwelling high salinity plumes, the distribution and geometry of which mirror those imaged in laboratory experiments of directional solidification of brine in a Hele-Shaw cell (Middleton et al., 2015). While the brinicle structures themselves do not house large salinity gradients, they form directly adjacent to regions that do (downwelling plumes). This is expected as brinicle formation is a result of the difference between thermal and molecular diffusivity in the system (Cartwright et al., 2013).

It is important to note, however, that brinicles on Earth only occur near land, in sheltered water where currents are low. Stronger currents induce turbulent mixing near the ice-ocean interface, dissipating the downwelling plumes and preventing brinicle formation. Given the substantial latitudinal currents predicted for icy satellites in the outer solar system (e.g. (Soderlund et al., 2014; Soderlund, 2019)) it is quite possible that brinicles may not be able to form. Conversely, the gradient rich brine channels within the mushy layer are protected from the underlying shear flow by the surrounding ice matrix. This suggests a putative ice-ocean interface habitat more akin to the terrestrial infaunal benthos rather than the extensional structures of chemical gardens. The importance of the ice-ocean interface as a potentially habitable environment on icy worlds as well as potential limitations of the current model in simulating brinicle geometry and evolution is discussed in Section 4 and Supplementary Section S4, respectively. Briefly, the implementation of Darcy’s law throughout the domain (Equation 2) will under predict fluid velocities in the underlying ocean, potentially impacting downwelling plume dynamics and altering the formation and evolution of brinicles, as these structures exist in and interact with the free fluid beneath the ice-ocean interface mushy layer.

## 4 Discussion

The ability to simulate, at high resolution, the two-dimensional evolution of Europa’s ice-ocean interface offers insight into the important role this boundary plays on icy worlds. A few examples are: the distribution of ocean-derived material within the ice shell; the relationship between impurity entrainment and ice-ocean interfacial thermal gradient; the

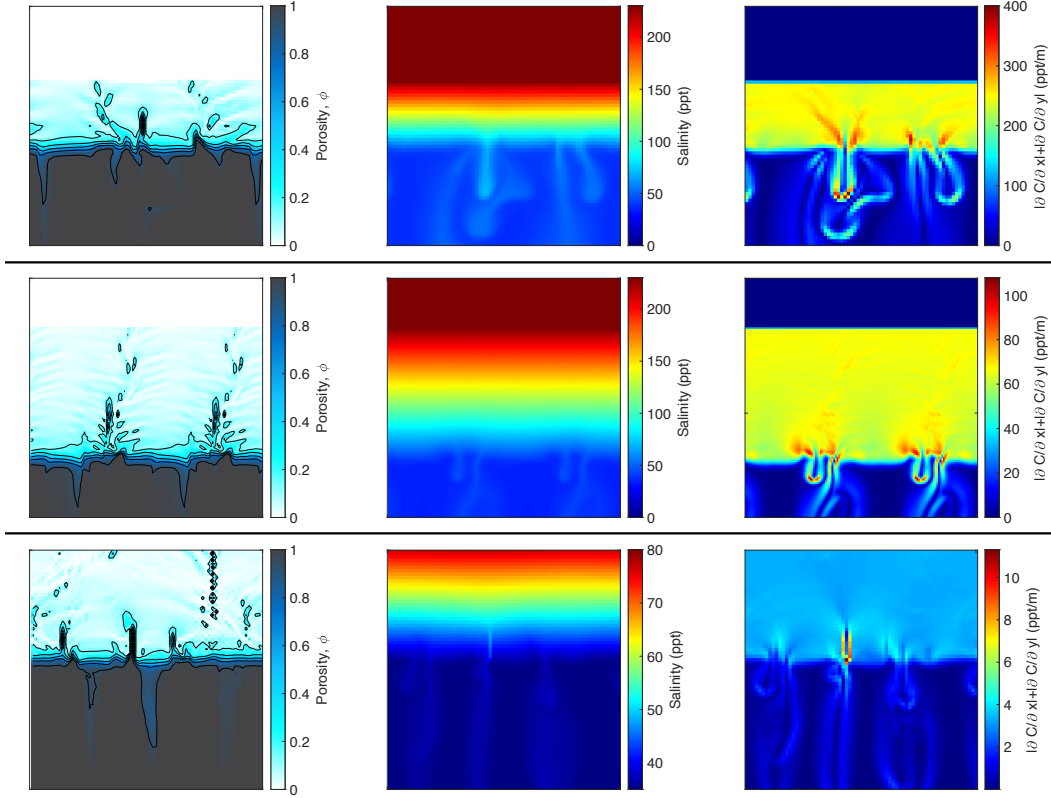


**Figure 6.** The physicochemical properties of brinicles on Europa. **(Top-Bottom)** Simulation results when the ice-ocean interface is at a depth of Top – 11 m (2.75 m x 2.75 m grid), Middle – 56 m (5.5 m x 5.5 m grid), and Bottom – 1084 m (27.5 m x 27.5 m grid). **(Left-Right)** Porosity (contours demarcate porosities of 0.15 to 0.95 in increments of 0.2), brine salinity, and absolute salinity gradient ( $|\partial C/\partial x| + |\partial C/\partial y|$ ) profiles during the simulations. (Note: the scale of the color bars differs between some of the images so as to highlight gradients within individual images. Additionally, these images have been extracted from simulations spanning much larger domains, ensuring the mushy layer is not impacted by edge effects.)

377 physicochemical structure of the ice-ocean interface; and the potential implications the ice-  
 378 ocean interface may have on habitability and geophysical processes.

379 Our work corroborates the work of Buffo et al. (2020) who implemented a one-dimensional  
 380 reactive transport model to predict the bulk salinity profile of Europa’s forming ice shell  
 381 and the evolution of hydrological structures within the shell. The functional relationship  
 382 between bulk salinity and depth within the ice shell derived by Buffo et al. (2020) captures  
 383 the structure of the bulk salinity profile simulated in this study (Figure 3a-c). In the shallow  
 384 shell substantial amounts of salt are retained in the forming ice, but as the ice shell thick-  
 385 enses salt is more efficiently drained from the mushy layer and bulk salinity asymptotically  
 386 approaches a nonzero lower limit. In congelation ice (ice formed due to conductive heat  
 387 loss to the overlying ice shell), such as we simulate here, this lower limit is governed by the  
 388 permeability of the mushy layer at low porosities. This is in contrast to marine ice (formed  
 389 by the buoyant deposition and compaction of ice crystals formed in the water column (Lewis  
 390 & Perkin, 1983; Buffo et al., 2021; Soderlund, 2019)), which more efficiently excludes so-  
 391 lutes and has been observed to have salinities an order of magnitude lower (J. Tison et  
 392 al., 2001). While an extremely important value in predicting the dynamics of the ice-ocean

393 interface, permeability, and its relationship to porosity, is not well constrained (Buffo et al.,  
 394 2020; Golden et al., 1998, 2007) and remains a contentious topic and active field of research  
 395 (Freitag & Eicken, 2003; McCarthy et al., 2013; Petrich et al., 2006). Reduced permeability  
 396 in the ice-ocean interfacial mushy layer or the existence of a percolation threshold below  
 397 a critical ice porosity (e.g. (Golden et al., 2007, 1998)) would result in amplified impurity  
 398 entrainment, while enhanced permeability would result in reduced impurity entrainment  
 399 (see Supplementary Section S1 and Figure S3). Similarly, our results show that at high  
 400 thermal gradients ( $>100$  K/m) ice effectively traps all of the salt from the parent liquid (i.e.  
 401 freezing is too rapid for salts to be expelled from the ice). Our results demonstrating the  
 402 relationship between salt entrainment and interfacial thermal gradient (Figure 3d-f) are an  
 403 improvement on the results of Buffo et al. (2020) whose one-dimensional model struggled  
 404 with stability issues under thermal gradients  $>20$  K/m.

405 We have shown that there exists a distinct and quantifiable relationship between the  
 406 thermochemical environment of the ice-ocean interface at the time of solidification and the  
 407 properties of the ice that forms. With the likelihood of ongoing hydrological activity within  
 408 Europa's ice shell in the form of lenses (B. E. Schmidt et al., 2011; Spaun et al., 1998),  
 409 sills (Chivers et al., 2020; Craft et al., 2016; Manga & Michaut, 2017; Michaut & Manga,  
 410 2014), dikes, fractures (Dombard et al., 2013; Rudolph & Manga, 2009; Walker et al., 2014),  
 411 and plumes (Jia et al., 2018; Sparks et al., 2016) understanding the characteristics of ice  
 412 formed in an array of thermal environments is imperative in constraining the mechanical,  
 413 dielectric, and eutectic properties of refrozen features. The presence of salt alters the rheo-  
 414 logical properties of ice (Assur, 1958; Durham et al., 2005; McCarthy et al., 2011) and could  
 415 facilitate the reactivation of fractures as well as the dynamics of solid-state convection in  
 416 the ductile portion of the ice shell (e.g. Buffo et al. (2020)). Shallow lenses within the shell  
 417 can be drastically affected by the dynamics of ice formation and salt entrainment/rejection.  
 418 Separated from the underlying ocean, progressive freezeout of these features results in con-  
 419 centration of the residual brine, depressing the freezing point of the fluid, increasing the  
 420 lens' longevity, and potentially resulting in the precipitation of salt hydrate layers when  
 421 the reservoir reaches saturation (Buffo et al., 2020; Chivers et al., 2020). Ice penetrating  
 422 radar observations depend critically on the dielectric properties of the ice shell (Di Paolo et  
 423 al., 2016; Kalousová et al., 2017; Moore, 2000), thus detecting and distinguishing features  
 424 within the ice shell as well as the ice-ocean interface relies on our understanding of the ice  
 425 shell's composition.

426 Any chemical measurements of plume particles (e.g. Cassini's measurements of Ence-  
 427 ladus' south polar plumes using the CDA (Hansen et al., 2011; Matson et al., 2007; Waite  
 428 et al., 2017)) rely on assumptions about the origin of the particles (ocean derived or sourced  
 429 from within the shell) and the quality of chemical signatures retained from the parent reser-  
 430 voir. Our results suggest that flash freezing at thermal gradients  $>100$  K/m would produce  
 431 ice particles that retain an exceptional chemical fingerprint of their parent fluid. However,  
 432 if plume particles form through a more temperate process (e.g. slow ascension through a  
 433 warm fracture (e.g. (J. Schmidt et al., 2008))) they may only preserve a fraction of the  
 434 source fluid's composition. If the thermal environment in the region of particle generation is  
 435 known, our results can be utilized to link particle chemistry observations to parent reservoir  
 436 chemistry. Lastly, any ocean-surface transport will be mediated by impurity entrainment  
 437 at the ice-ocean interface (Allu Peddinti & McNamara, 2015). Thus, constraining materi-  
 438 al entrainment rates is crucial to assessing the fluxes associated with potential chemical  
 439 overturn within the ice shell that may facilitate disequilibrium chemistries favorable for life  
 440 (Hand et al., 2007; Vance et al., 2016) and will govern observable biosignature delivery to  
 441 the surface/upper ice shell (B. E. Schmidt, 2020).

442 Although there are important parallels between the ice-ocean interfaces of icy worlds  
 443 and those found on Earth beneath sea ice and ice shelves (e.g. (Buffo et al., 2020; Greeley et  
 444 al., 1998; Pappalardo & Coon, 1996)), there are important facets of their scale and structure  
 445 which may facilitate unique processes not represented in terrestrial analog systems. For

446 Europa, the thickness of the ice shell ( $\sim 10\text{-}30$  km) coupled with a gravity approximately  
 447 one tenth that of Earth ( $\sim 1.32$  m/s<sup>2</sup>) leads to predicted ice-ocean interface mushy layer  
 448 thicknesses of 537 m and 1611 m for a 10 km and 30 km thick ice shell, respectively (using  
 449 equation 11 and the coefficients given in the caption of Figure 5). These thicknesses far  
 450 exceed the  $\sim 10\text{-}30$  cm thick mushy layers observed in sea ice (Feltham et al., 2006; Hunke et  
 451 al., 2011; Worster & Rees Jones, 2015) and meters to tens of meters of hydraulic connectivity  
 452 observed at the base of ice shelves (Craven et al., 2009; Zotikov et al., 1980). Moreover, if  
 453 there exist other ocean impurities that further depress its eutectic temperature the ice-ocean  
 454 interface mushy layer could be even thicker. It is important to note that these mushy layer  
 455 thickness predictions are associated with an actively growing ice shell. It is possible that  
 456 contemporary ice shells have reached a quasi-equilibrium thermal state (e.g. (Husmann et  
 457 al., 2002)) in which temporal and spatial patterns of thickening and thinning have conspired  
 458 to produce a heterogeneous mushy layer (or lack thereof in regions which are thinning or  
 459 have reached an equilibrium thickness) (Buffo et al., 2021). This has important implications  
 460 for the geophysics and astrobiological potential of ice-ocean interface environments, a full  
 461 account of which can be found in (Buffo et al., 2021).

462 With the likely global nature of Europa’s ice-ocean interface, and its adjacency to the  
 463 moon’s ductile, likely convective, icy mantle (Barr & McKinnon, 2007; Han & Showman,  
 464 2005; McKinnon, 1999), we suggest that in a number of aspects it may be best thought of as  
 465 a core-mantle phase boundary, akin to the D” layer of Earth. Existing as a multiphase layer,  
 466 separating a denser fluid underlying a lighter solid (outer core and mantle, respectively),  
 467 this elusive layer plays an integral role in Earth’s geophysical evolution (Burke et al., 2008;  
 468 Maruyama et al., 2007; Olson et al., 1987). In this analogy, regional topography and  
 469 heterogeneous heat flow could drive ice dynamics mirroring diapiric mantle plumes and  
 470 tectonic processes on Earth (Burke et al., 2008; Lay et al., 2008; Olson et al., 1987), both  
 471 of which have been suggested by geomorphological observations of features on Europa’s  
 472 surface (Head et al., 1999; Kattenhorn & Hurford, 2009; Kattenhorn & Prockter, 2014;  
 473 Pappalardo & Barr, 2004; Prockter et al., 2002; B. E. Schmidt et al., 2011). If this is  
 474 the case, the multiphase ice-ocean boundary of Europa not only governs the rates of heat  
 475 and mass transport between the two reservoirs via micro- and mesoscopic physics but may  
 476 also dictate regional and global scale geophysical processes. With the importance the D”  
 477 layer plays in magmatic and tectonic processes on Earth, and analogous cryovolcanism (ice  
 478 shell hydrology) (Fagents et al., 2000; Sparks et al., 2017) and ice tectonism (Kattenhorn &  
 479 Hurford, 2009; Kattenhorn & Prockter, 2014) likely occurring on Europa, constraining the  
 480 structure and heterogeneity of the ice-ocean interface mushy layer promises to provide novel  
 481 insight on the dynamics and evolution of icy worlds. Additionally, and perhaps surprisingly,  
 482 the ice-ocean interface of Europa provides a more accessible (See NASA’s SESAME project  
 483 (Howell & Pappalardo, 2020)) analog of the terrestrial D” layer and could be used to explore  
 484 hypotheses regarding the Earth’s interior.

485 The porous and reactive nature of the ice-ocean interface would provide an exceptional  
 486 niche for any biology in the oceans of icy satellites. As the location where surface derived  
 487 oxidants would be introduced into the theoretically reduced ocean (Hand et al., 2007; Vance  
 488 et al., 2016), the ice-ocean boundary layer of Europa would be rich in chemical gradients  
 489 and disequilibria in an otherwise likely oligotrophic water column (less the ocean-rock in-  
 490 terface  $\sim 100$  km below) (Lipps & Rieboldt, 2005). This is in addition to the chemical  
 491 gradients produced by ice formation (e.g. Section 3.3). On Earth, the basal surfaces of  
 492 oceanic ices (sea ice, ice shelves) house a rich community of bacteria, algae and higher order  
 493 heterotrophs (Daly et al., 2013; Gradinger et al., 1999; Loose et al., 2011; Spindler,  
 494 1994; Thomas & Dieckmann, 2003). On icy worlds, devoid of sunlight, any biotic systems  
 495 will likely be fueled by chemolithoautotrophic primary producers (Hoover & Pikuta, 2010;  
 496 Pikuta & Hoover, n.d.; B. E. Schmidt, 2020), similar to hydrothermal, deep benthic, and/or  
 497 endolithic environments on Earth. In thick ice shells with permeable layers  $>1$  km thick  
 498 there may be an array of unique ice-ocean/brine sub-environments within these layers which  
 499 could be colonized by extremophiles adapted to take advantage of regional sources of en-

500 ergy. With Europa’s prominence amongst high priority astrobiology targets constraining  
 501 the physicochemical dynamics and habitability of a long-lived (in comparison to shallow  
 502 features) and accessible (in comparison to the seafloor) biologically favorable niche is in line  
 503 with a multitude of NASA goals (NRC, 2012; Des Marais et al., 2008; Hendrix et al., 2019).

## 504 5 Conclusion

505 The ice-ocean interface of Europa and other icy worlds is likely characterized by a  
 506 dynamic mushy zone consisting of porous ice and saline interstitial brine. Such reactive phase  
 507 change boundaries play an integral role in both the biogeochemical cycling and geophysics  
 508 of the Earth (Loose et al., 2011; Hunke et al., 2011). Similarly, as a likely ubiquitous feature  
 509 on Europa and other icy satellites the ice-ocean interface dictates ocean-surface transport,  
 510 the physicochemical characteristics of the ice shell, likely governs both regional and global  
 511 geophysical processes, and may provide a gradient rich oasis for any resident organisms.  
 512 Constraining the dynamics and properties of the ice-ocean interface will improve geophysical  
 513 models of the ice shell, aid in the planning and synthesis of missions in the lens of planetary  
 514 exploration and planetary protection directives, and help constrain the habitability of ice-  
 515 ocean worlds.

## 516 Acknowledgments

517 *Data Availability Statement:* SOFTBALL and its associated documentation can be found in  
 518 (J. R. G. Parkinson, Martin, & Buffo, 2020). All model input files used in this manuscript  
 519 can be found in the repository directory ‘mushy-layer/examples/europa’ (J. R. G. Parkinson,  
 520 Martin, & Buffo, 2020).

## 521 References

- 522 Ackley, S. F., & Sullivan, C. W. (1994). Physical controls on the development and charac-  
 523 teristics of antarctic sea ice biological communities—a review and synthesis [Journal  
 524 Article]. *Deep Sea Research Part I: Oceanographic Research Papers*, *41*(10), 1583-  
 525 1604.
- 526 Allu Peddinti, D., & McNamara, A. K. (2015). Material transport across europa’s ice shell  
 527 [Journal Article]. *Geophysical Research Letters*, *42*(11), 4288-4293.
- 528 Assur, A. (1958). Composition of sea ice and its tensile strength [Journal Article]. *Arctic*  
 529 *sea ice*, *598*, 106-138.
- 530 Barge, L. M., Abedian, Y., Doloboff, I. J., Nuñez, J. E., Russell, M. J., Kidd, R. D., & Kanik,  
 531 I. (2015). Chemical gardens as flow-through reactors simulating natural hydrothermal  
 532 systems [Journal Article]. *JoVE (Journal of Visualized Experiments)*(105), e53015.
- 533 Barr, A. C., & McKinnon, W. B. (2007). Convection in ice i shells and mantles with  
 534 self-consistent grain size [Journal Article]. *Journal of Geophysical Research: Planets*,  
 535 *112*(E2).
- 536 Bear, J. (2013). *Dynamics of fluids in porous media* [Book]. Courier Corporation.
- 537 Bierson, C. J., Nimmo, F., & Stern, S. A. (2020). Evidence for a hot start and early ocean  
 538 formation on pluto [Journal Article]. *Nature Geoscience*. Retrieved from [https://](https://doi.org/10.1038/s41561-020-0595-0)  
 539 [doi.org/10.1038/s41561-020-0595-0](https://doi.org/10.1038/s41561-020-0595-0) doi: 10.1038/s41561-020-0595-0
- 540 Brown, E. K., Buffo, J. J., Grantham, M., Pontefract, A., Glass, J., Ingall, E., . . . Carr,  
 541 C. (2020). Trapped in the ice: An analysis of brines in british columbia’s hypersaline  
 542 lakes [Journal Article]. *LPI(2326)*, 2218.
- 543 Buffo, J. J. (2019). *Multiphase reactive transport in planetary ices* (Thesis). Georgia  
 544 Institute of Technology.
- 545 Buffo, J. J., Schmidt, B. E., Huber, C., & Meyer, C. R. (2021). Characterizing the ice-  
 546 ocean interface of icy worlds: A theoretical approach. *Icarus*. doi: 10.1016/j.icarus  
 547 .2021.114318

- 548 Buffo, J. J., Schmidt, B. E., Huber, C., & Walker, C. C. (2020). Entrainment and dynamics  
549 of ocean-derived impurities within europa’s ice shell [Journal Article]. *JGR: Planets*.
- 550 Burke, K., Steinberger, B., Torsvik, T. H., & Smethurst, M. A. (2008). Plume generation  
551 zones at the margins of large low shear velocity provinces on the core–mantle boundary  
552 [Journal Article]. *Earth and Planetary Science Letters*, *265*(1-2), 49-60.
- 553 Cartwright, J. H. E., Escribano, B., González, D. L., Sainz-Díaz, C. I., & Tuval, I. (2013).  
554 Brinicles as a case of inverse chemical gardens [Journal Article]. *Langmuir*, *29*(25),  
555 7655-7660.
- 556 Cartwright, J. H. E., García-Ruiz, J. M., Novella, M. L., & Otálora, F. (2002). Formation  
557 of chemical gardens [Journal Article]. *Journal of colloid and interface science*, *256*(2),  
558 351-359.
- 559 Chivers, C. J., Buffo, J. J., & Schmidt, B. E. (2020). Thermal and chemical evolution of  
560 small, shallow water bodies on europa [Journal Article]. *LPI(2326)*, 1047.
- 561 Chung, C., & Worster, M. G. (2002). Steady-state chimneys in a mushy layer [Journal  
562 Article]. *Journal of Fluid Mechanics*, *455*, 387.
- 563 Cottier, F., Eicken, H., & Wadhams, P. (1999). Linkages between salinity and brine chan-  
564 nel distribution in young sea ice [Journal Article]. *Journal of Geophysical Research:  
565 Oceans*, *104*(C7), 15859-15871.
- 566 Cox, G. F. N., & Weeks, W. F. (1974). Salinity variations in sea ice [Journal Article].  
567 *Journal of Glaciology*, *13*(67), 109-120.
- 568 Craft, K. L., Patterson, G. W., Lowell, R. P., & Germanovich, L. (2016). Fracturing and  
569 flow: Investigations on the formation of shallow water sills on europa [Journal Article].  
570 *Icarus*, *274*, 297-313.
- 571 Craven, M., Allison, I., Fricker, H. A., & Warner, R. (2009). Properties of a marine ice layer  
572 under the amery ice shelf, east antarctica [Journal Article]. *Journal of Glaciology*,  
573 *55*(192), 717-728.
- 574 Daly, M., Rack, F., & Zook, R. (2013). *Edwardsiella andrillae*, a new species of sea anemone  
575 from antarctic ice [Journal Article]. *PloS one*, *8*(12), e83476.
- 576 Des Marais, D. J., Nuth, J. A., Allamandola, L. J., Boss, A. P., Farmer, J. D., Hoehler,  
577 T. M., ... Runnegar, B. (2008). The nasa astrobiology roadmap [Journal Article].  
578 *Astrobiology*, *8*(4), 715-730.
- 579 Di Paolo, F., Lauro, S. E., Castelletti, D., Mitri, G., Bovolo, F., Cosciotti, B., ... Bruz-  
580 zone, L. (2016). Radar signal penetration and horizons detection on europa through  
581 numerical simulations [Journal Article]. *IEEE Journal of Selected Topics in Applied  
582 Earth Observations and Remote Sensing*, *10*(1), 118-129.
- 583 Dombard, A. J., Patterson, G. W., Lederer, A. P., & Prockter, L. M. (2013). Flanking  
584 fractures and the formation of double ridges on europa [Journal Article]. *Icarus*,  
585 *223*(1), 74-81.
- 586 Durham, W. B., Stern, L. A., Kubo, T., & Kirby, S. H. (2005). Flow strength of highly  
587 hydrated mg-and na-sulfate hydrate salts, pure and in mixtures with water ice, with  
588 application to europa [Journal Article]. *Journal of Geophysical Research: Planets*,  
589 *110*(E12).
- 590 Eicken, H. (1992). Salinity profiles of antarctic sea ice: field data and model results [Journal  
591 Article]. *Journal of Geophysical Research: Oceans*, *97*(C10), 15545-15557.
- 592 Fagents, S. A., Greeley, R., Sullivan, R. J., Pappalardo, R. T., Prockter, L. M., & Team,  
593 G. S. (2000). Cryomagmatic mechanisms for the formation of rhadamanthys lineae,  
594 triple band margins, and other low-albedo features on europa [Journal Article]. *Icarus*,  
595 *144*(1), 54-88.
- 596 Feltham, D. L., Untersteiner, N., Wettlaufer, J. S., & Worster, M. G. (2006). Sea ice is a  
597 mushy layer [Journal Article]. *Geophysical Research Letters*, *33*(14).
- 598 Fortes, A. D. (2000). Exobiological implications of a possible ammonia–water ocean inside  
599 titan [Journal Article]. *Icarus*, *146*(2), 444-452.
- 600 Freitag, J., & Eicken, H. (2003). Meltwater circulation and permeability of arctic summer sea  
601 ice derived from hydrological field experiments [Journal Article]. *Journal of Glaciology*,  
602 *49*(166), 349-358.

- 603 Golden, K. M., Ackley, S. F., & Lytle, V. (1998). The percolation phase transition in sea  
604 ice [Journal Article]. *Science*, *282*(5397), 2238-2241.
- 605 Golden, K. M., Eicken, H., Heaton, A. L., Miner, J., Pringle, D. J., & Zhu, J. (2007).  
606 Thermal evolution of permeability and microstructure in sea ice [Journal Article].  
607 *Geophysical Research Letters*, *34*(16).
- 608 Gradinger, R., Friedrich, C., & Spindler, M. (1999). Abundance, biomass and composition  
609 of the sea ice biota of the greenland sea pack ice [Journal Article]. *Deep Sea Research*  
610 *Part II: Topical Studies in Oceanography*, *46*(6-7), 1457-1472.
- 611 Grasset, O., Dougherty, M. K., Coustenis, A., Bunce, E. J., Erd, C., Titov, D., . . . Fletcher,  
612 L. N. (2013). Jupiter icy moons explorer (juice): An esa mission to orbit ganymede  
613 and to characterise the jupiter system [Journal Article]. *Planetary and Space Science*,  
614 *78*, 1-21.
- 615 Greeley, R., Sullivan, R., Coon, M. D., Geissler, P. E., Tufts, B. R., Head III, J. W.,  
616 . . . Moore, J. M. (1998). Terrestrial sea ice morphology: Considerations for europa  
617 [Journal Article]. *Icarus*, *135*(1), 25-40.
- 618 Hammond, N. P., Barr, A. C., & Parmentier, E. M. (2016). Recent tectonic activity on  
619 pluto driven by phase changes in the ice shell [Journal Article]. *Geophysical Research*  
620 *Letters*, *43*(13), 6775-6782.
- 621 Hammond, N. P., Parmentier, E., & Barr, A. C. (2018). Compaction and melt transport  
622 in ammonia-rich ice shells: Implications for the evolution of triton [Journal Article].  
623 *Journal of Geophysical Research: Planets*, *123*(12), 3105-3118.
- 624 Han, L., & Showman, A. P. (2005). Thermo-compositional convection in europa's icy shell  
625 with salinity [Journal Article]. *Geophysical research letters*, *32*(20).
- 626 Hand, K. P., Carlson, R. W., & Chyba, C. F. (2007). Energy, chemical disequilibrium, and  
627 geological constraints on europa [Journal Article]. *Astrobiology*, *7*(6), 1006-1022.
- 628 Hand, K. P., Chyba, C., Priscu, J., Carlson, R., & Nealson, K. (2009). Astrobiology and  
629 the potential for life on europa [Journal Article]. *Europa*, 589-629.
- 630 Hand, K. P., & Chyba, C. F. (2007). Empirical constraints on the salinity of the european  
631 ocean and implications for a thin ice shell [Journal Article]. *Icarus*, *189*(2), 424-438.
- 632 Hansen, C., Shemansky, D. E., Esposito, L. W., Stewart, A., Lewis, B., Colwell, J., . . .  
633 Teolis, B. (2011). The composition and structure of the enceladus plume [Journal  
634 Article]. *Geophysical Research Letters*, *38*(11).
- 635 Head, J. W., Pappalardo, R. T., & Sullivan, R. (1999). Europa: Morphological charac-  
636 teristics of ridges and triple bands from galileo data (e4 and e6) and assessment of a  
637 linear diapirism model [Journal Article]. *Journal of Geophysical Research: Planets*,  
638 *104*(E10), 24223-24236.
- 639 Hendrix, A. R., Hurford, T. A., Barge, L. M., Bland, M. T., Bowman, J. S., Brinckerhoff,  
640 W., . . . Collins, G. C. (2019). The nasa roadmap to ocean worlds [Journal Article].  
641 *Astrobiology*, *19*(1), 1-27.
- 642 Hoover, R. B., & Pikuta, E. V. (2010). Psychrophilic and psychrotolerant microbial ex-  
643 tremophiles in polar environments [Journal Article].
- 644 Howell, S. M., & Pappalardo, R. T. (2018). Band formation and ocean-surface interaction  
645 on europa and ganymede [Journal Article]. *Geophysical Research Letters*, *45*(10),  
646 4701-4709.
- 647 Howell, S. M., & Pappalardo, R. T. (2020). Nasa's europa clipper—a mission to a potentially  
648 habitable ocean world [Journal Article]. *Nature Communications*, *11*(1), 1-4.
- 649 Hunke, E., Notz, D., Turner, A., & Vancoppenolle, M. (2011). The multiphase physics of sea  
650 ice: a review for model developers [Journal Article]. *The Cryosphere*, *5*(4), 989-1009.
- 651 Hussmann, H., Spohn, T., & Wiczerkowski, K. (2002). Thermal equilibrium states  
652 of europa's ice shell: Implications for internal ocean thickness and surface heat  
653 flow [Journal Article]. *Icarus*, *156*(1), 143-151. Retrieved from <GotoISI>://WOS:  
654 000175374300009 doi: 10.1006/icar.2001.6776
- 655 Jia, X., Kivelson, M. G., Khurana, K. K., & Kurth, W. S. (2018). Evidence of a plume on  
656 europa from galileo magnetic and plasma wave signatures [Journal Article]. *Nature*  
657 *Astronomy*, *2*(6), 459-464.

- 658 Johnson, B. C., Sheppard, R. Y., Pascuzzo, A. C., Fisher, E. A., & Wiggins, S. E. (2017).  
659 Porosity and salt content determine if subduction can occur in europa’s ice shell [Journal  
660 Article]. *Journal of Geophysical Research: Planets*, *122*(12), 2765-2778.
- 661 Kalousova, K., Schroeder, D. M., & Soderlund, K. M. (2017). Radar attenuation in europa’s  
662 ice shell: Obstacles and opportunities for constraining the shell thickness and its  
663 thermal structure [Journal Article]. *Journal of Geophysical Research: Planets*, *122*(3),  
664 524-545.
- 665 Karani, H., & Huber, C. (2017). Transitional behaviour of convective patterns in free  
666 convection in porous media [Journal Article]. *Journal of Fluid Mechanics*, *818*.
- 667 Kargel, J. S., Kaye, J. Z., Head III, J. W., Marion, G. M., Sassen, R., Crowley, J. K., ...  
668 Hogenboom, D. L. (2000). Europa’s crust and ocean: origin, composition, and the  
669 prospects for life [Journal Article]. *Icarus*, *148*(1), 226-265.
- 670 Kattenhorn, S. A., & Hurford, T. (2009). Tectonics of europa [Book Section]. In *Europa*  
671 (p. 199-236). University of Arizona Press Tucson.
- 672 Kattenhorn, S. A., & Prockter, L. M. (2014). Evidence for subduction in the ice shell of  
673 europa [Journal Article]. *Nature Geoscience*, *7*(10), 762.
- 674 Katz, R. F., & Worster, M. G. (2008). Simulation of directional solidification, thermochem-  
675 ical convection, and chimney formation in a hele-shaw cell [Journal Article]. *Journal*  
676 *of Computational Physics*, *227*(23), 9823-9840.
- 677 Khurana, K., Kivelson, M., Stevenson, D., Schubert, G., Russell, C., Walker, R., &  
678 Polanskey, C. (1998). Induced magnetic fields as evidence for subsurface oceans  
679 in europa and callisto [Journal Article]. *Nature*, *395*(6704), 777.
- 680 Kirk, R. L., Brown, R. H., & Soderblom, L. A. (1990). Subsurface energy storage and  
681 transport for solar-powered geysers on triton [Journal Article]. *Science*, *250*(4979),  
682 424-429.
- 683 Lay, T., Hernlund, J., & Buffett, B. A. (2008). Core–mantle boundary heat flow [Journal  
684 Article]. *Nature geoscience*, *1*(1), 25.
- 685 Le Bars, M., & Worster, M. G. (2006). Interfacial conditions between a pure fluid and a  
686 porous medium: implications for binary alloy solidification [J. Fluid Mech.].
- 687 Lewis, E. L., & Perkin, R. G. (1983). Supercooling and energy exchange near the arctic  
688 ocean surface [Journal Article]. *Journal of Geophysical Research-Oceans*, *88*(Nc12),  
689 7681-7685. Retrieved from <Go to ISI>://WOS:A1983RG83200017 doi: DOI10.1029/  
690 JC088iC12p07681
- 691 Lipps, J. H., & Rieboldt, S. (2005). Habitats and taphonomy of europa [Journal Article].  
692 *Icarus*, *177*(2), 515-527.
- 693 Loose, B., Miller, L. A., Elliott, S., & Papakyriakou, T. (2011). Sea ice biogeochemistry and  
694 material transport across the frozen interface [Journal Article]. *Oceanography*, *24*(3),  
695 202-218.
- 696 Mahadevan, K. (2017). *The growth and dynamics of brinicles* (Undergraduate Thesis).  
697 School of Engineering and Applied Sciences, Harvard University.
- 698 Manga, M., & Michaut, C. (2017). Formation of lenticulae on europa by saucer-shaped sills  
699 [Journal Article]. *Icarus*, *286*, 261-269.
- 700 Marion, G. M., Fritsen, C. H., Eicken, H., & Payne, M. C. (2003). The search for life  
701 on europa: limiting environmental factors, potential habitats, and earth analogues  
702 [Journal Article]. *Astrobiology*, *3*(4), 785-811.
- 703 Maruyama, S., Santosh, M., & Zhao, D. (2007). Superplume, supercontinent, and post-  
704 perovskite: mantle dynamics and anti-plate tectonics on the core–mantle boundary  
705 [Journal Article]. *Gondwana Research*, *11*(1-2), 7-37.
- 706 Matson, D. L., Castillo, J. C., Lunine, J., & Johnson, T. V. (2007). Enceladus’ plume:  
707 Compositional evidence for a hot interior [Journal Article]. *Icarus*, *187*(2), 569-573.
- 708 McCarthy, C., Blackford, J., & Jeffree, C. (2013). Low-temperature-SEM study of dihedral  
709 angles in the ice-i/sulfuric acid partially molten system [Journal Article]. *Journal of*  
710 *microscopy*, *249*(2), 150-157.
- 711 McCarthy, C., Cooper, R. F., Goldsby, D. L., Durham, W. B., & Kirby, S. H. (2011). Tran-  
712 sient and steady state creep response of ice i and magnesium sulfate hydrate eutectic

- 713 aggregates [Journal Article]. *Journal of Geophysical Research: Planets*, 116(E4).
- 714 McCarthy, C., Cooper, R. F., Kirby, S. H., Rieck, K. D., & Stern, L. A. (2007). Solidifica-  
715 tion and microstructures of binary ice-i/hydrate eutectic aggregates [Journal Article].  
716 *American Mineralogist*, 92(10), 1550-1560.
- 717 McKinnon, W. B. (1999). Convective instability in europa's floating ice shell [Journal  
718 Article]. *Geophysical Research Letters*, 26(7), 951-954.
- 719 McKinnon, W. B., & Kirk, R. L. (2014). Triton [Book Section]. In *Encyclopedia of the*  
720 *solar system* (p. 861-881). Elsevier.
- 721 Michaut, C., & Manga, M. (2014). Domes, pits, and small chaos on europa produced  
722 by water sills [Journal Article]. *Journal of Geophysical Research: Planets*, 119(3),  
723 550-573.
- 724 Middleton, C., Thomas, C., Escala, D., Tison, J.-L., & De Wit, A. (2015). Imaging the  
725 evolution of brine transport in experimentally grown quasi-two-dimensional sea ice  
726 [Journal Article]. *Procedia IUTAM*, 15, 95-100.
- 727 Moore, J. C. (2000). Models of radar absorption in european ice [Journal Article]. *Icarus*,  
728 147(1), 292-300.
- 729 Nakawo, M., & Sinha, N. K. (1981). Growth rate and salinity profile of first-year sea ice in  
730 the high arctic [Journal Article]. *Journal of Glaciology*, 27(96), 315-330.
- 731 Nimmo, F. (2020). Solving the puzzle of enceladus's active south pole [Journal Article].  
732 *Proceedings of the National Academy of Sciences*, 117(28), 16107-16108.
- 733 Nimmo, F., & Pappalardo, R. (2016). Ocean worlds in the outer solar system [Journal  
734 Article]. *Journal of Geophysical Research: Planets*, 121(8), 1378-1399.
- 735 Notz, D., Wettlaufer, J. S., & Worster, M. G. (2005). A non-destructive method for  
736 measuring the salinity and solid fraction of growing sea ice in situ [Journal Article].  
737 *Journal of Glaciology*, 51(172), 159-166.
- 738 NRC. (2012). *Vision and voyages for planetary science in the decade 2013-2022* [Book].  
739 National Academies Press.
- 740 Olson, P., Schubert, G., & Anderson, C. (1987). Plume formation in the d"-layer and the  
741 roughness of the core-mantle boundary [Journal Article]. *Nature*, 327(6121), 409.
- 742 Pappalardo, R. T., & Barr, A. C. (2004). The origin of domes on europa: The role of  
743 thermally induced compositional diapirism [Journal Article]. *Geophysical Research*  
744 *Letters*, 31(1).
- 745 Pappalardo, R. T., & Coon, M. (1996). A sea ice analog for the surface of europa [Conference  
746 Proceedings]. In *Lunar and planetary science conference* (Vol. 27).
- 747 Pappalardo, R. T., Senske, D., Korth, H., Klima, R., Vance, S., & Craft, K. (2017). The  
748 europa clipper mission: Exploring the habitability of a unique icy world [Conference  
749 Proceedings]. In *European planetary science congress* (Vol. 11).
- 750 Parkinson, C. D., Liang, M.-C., Yung, Y. L., & Kirschvink, J. L. (2008). Habitability of  
751 enceladus: planetary conditions for life [Journal Article]. *Origins of Life and Evolution*  
752 *of Biospheres*, 38(4), 355-369.
- 753 Parkinson, J. R. G. (2019). *Nonlinear convection in sea ice and other mushy layers* (Thesis).  
754 University of Oxford.
- 755 Parkinson, J. R. G., Martin, D., & Buffo, J. (2020, October). *jrgparkinson/mushy-layer:*  
756 *Code and input files for Europa simulations*. Zenodo. Retrieved from [https://doi](https://doi.org/10.5281/zenodo.4118549)  
757 [.org/10.5281/zenodo.4118549](https://doi.org/10.5281/zenodo.4118549) doi: 10.5281/zenodo.4118549
- 758 Parkinson, J. R. G., Martin, D. F., Wells, A. J., & Katz, R. F. (2020). Modelling bi-  
759 nary alloy solidification with adaptive mesh refinement [Journal Article]. *Journal of*  
760 *Computational Physics: X*, 5, 100043.
- 761 Petrich, C., Langhorne, P. J., & Sun, Z. F. (2006). Modelling the interrelationships between  
762 permeability, effective porosity and total porosity in sea ice [Journal Article]. *Cold*  
763 *Regions Science and Technology*, 44(2), 131-144.
- 764 Pikuta, E. V., & Hoover, R. B. (n.d.). Astrobiological significance of chemolithoautotrophic  
765 acidophiles [Conference Proceedings]. In *Instruments, methods, and missions for as-*  
766 *trobiology vii* (Vol. 5163, p. 179-190). International Society for Optics and Photonics.
- 767 Porco, C., Helfenstein, P., Thomas, P., Ingersoll, A., Wisdom, J., West, R., ... Roatsch, T.

- 768 (2006). Cassini observes the active south pole of enceladus [Journal Article]. *science*,  
769 *311*(5766), 1393-1401.
- 770 Prockter, L. M., Head, J. W., Pappalardo, R. T., Sullivan, R. J., Clifton, A. E., Giese, B.,  
771 ... Neukum, G. (2002). Morphology of european bands at high resolution: A mid-  
772 ocean ridge-type rift mechanism [Journal Article]. *Journal of Geophysical Research:*  
773 *Planets*, *107*(E5).
- 774 Rees Jones, D. W., & Worster, M. G. (2013). A simple dynamical model for gravity drainage  
775 of brine from growing sea ice [Journal Article]. *Geophysical Research Letters*, *40*(2),  
776 307-311.
- 777 Rudolph, M. L., & Manga, M. (2009). Fracture penetration in planetary ice shells [Journal  
778 Article]. *Icarus*, *199*(2), 536-541.
- 779 Santibáñez, P. A., Michaud, A. B., Vick-Majors, T. J., D'Andrilli, J., Chiuchiolo, A., Hand,  
780 K. P., & Priscu, J. C. (2019). Differential incorporation of bacteria, organic matter,  
781 and inorganic ions into lake ice during ice formation [Journal Article]. *Journal of*  
782 *Geophysical Research: Biogeosciences*.
- 783 Schmidt, B. E. (2020). The astrobiology of europa and the jovian system [Journal Article].  
784 *Planetary Astrobiology*, 185.
- 785 Schmidt, B. E., Blankenship, D., Patterson, G., & Schenk, P. (2011). Active formation  
786 of 'chaos terrain' over shallow subsurface water on europa [Journal Article]. *Nature*,  
787 *479*(7374), 502.
- 788 Schmidt, B. E., Buffo, J., & Main Campus, A. (n.d.). Biomarker production and preservation  
789 on europa [Conference Proceedings]. In *European planetary science congress* (Vol. 11).
- 790 Schmidt, J., Brilliantov, N., Spahn, F., & Kempf, S. (2008). Slow dust in enceladus' plume  
791 from condensation and wall collisions in tiger stripe fractures [Journal Article]. *Nature*,  
792 *451*(7179), 685-688.
- 793 Schroeder, D. M., Romero-Wolf, A., Carrer, L., Grima, C., Campbell, B. A., Kofman, W.,  
794 ... Blankenship, D. D. (2016). Assessing the potential for passive radio sounding of  
795 europa and ganymede with rime and reason [Journal Article]. *Planetary and Space*  
796 *Science*, *134*, 52-60.
- 797 Schubert, G., Anderson, J., Spohn, T., & McKinnon, W. (2004). Interior composition,  
798 structure and dynamics of the galilean satellites [Journal Article]. *Jupiter: The planet,*  
799 *satellites and magnetosphere*, *1*, 281-306.
- 800 Soderlund, K. M. (2019). Ocean dynamics of outer solar system satellites [Journal Article].  
801 *Geophysical Research Letters*, *46*(15), 8700-8710. Retrieved from <Go to ISI>://WOS:  
802 000483812500013 doi: 10.1029/2018gl081880
- 803 Soderlund, K. M., Schmidt, B. E., Wicht, J., & Blankenship, D. D. (2014). Ocean-driven  
804 heating of europa's icy shell at low latitudes [Journal Article]. *Nature Geoscience*, *7*(1),  
805 16-19. Retrieved from <Go to ISI>://WOS:000328962700012 doi: 10.1038/Ngeo2021
- 806 Sotin, C., Head III, J. W., & Tobie, G. (2002). Europa: Tidal heating of upwelling thermal  
807 plumes and the origin of lenticulae and chaos melting [Journal Article]. *Geophysical*  
808 *Research Letters*, *29*(8), 74-1-74-4.
- 809 Sparks, W. B., Hand, K., McGrath, M., Bergeron, E., Cracraft, M., & Deustua, S. (2016).  
810 Probing for evidence of plumes on europa with hst/stis [Journal Article]. *The Astro-*  
811 *physical Journal*, *829*(2), 121.
- 812 Sparks, W. B., Schmidt, B. E., McGrath, M. A., Hand, K. P., Spencer, J. R., Cracraft,  
813 M., & Deustua, S. E. (2017). Active cryovolcanism on europa? [Journal Article]. *The*  
814 *Astrophysical Journal Letters*, *839*(2), L18.
- 815 Spaun, N., Head, J., Collins, G., Prockter, L., & Pappalardo, R. (1998). Conamara chaos  
816 region, europa: Reconstruction of mobile polygonal ice blocks [Journal Article]. *Geo-*  
817 *physical research letters*, *25*(23), 4277-4280.
- 818 Spindler, M. (1994). Notes on the biology of sea ice in the arctic and antarctic [Journal  
819 Article]. *Polar Biology*, *14*(5), 319-324.
- 820 Steefel, C. I., DePaolo, D. J., & Lichtner, P. C. (2005). Reactive transport modeling: An  
821 essential tool and a new research approach for the earth sciences [Journal Article].  
822 *Earth and Planetary Science Letters*, *240*(3-4), 539-558.

- 823 Tedesco, L., & Vichi, M. (2014). Sea ice biogeochemistry: A guide for modellers [Journal  
824 Article]. *PLoS one*, *9*(2), e89217.
- 825 Thomas, D. N., & Dieckmann, G. S. (2003). Biogeochemistry of antarctic sea ice [Book  
826 Section]. In *Oceanography and marine biology, an annual review, volume 40* (p. 151-  
827 156). CRC Press.
- 828 Thomas, D. N., & Dieckmann, G. S. (2008). *Sea ice: an introduction to its physics,*  
829 *chemistry, biology and geology* [Book]. John Wiley & Sons.
- 830 Tison, J., Khazendar, A., & Roulin, E. (2001). A two-phase approach to the simulation  
831 of the combined isotope/salinity signal of marine ice [Journal Article]. *Journal of*  
832 *Geophysical Research: Oceans*, *106*(C12), 31387-31401.
- 833 Tison, J.-L., & Verbeke, V. (2001). Chlorinity/salinity distribution patterns in experimental  
834 granular sea ice [Journal Article]. *Annals of Glaciology*, *33*, 13-20.
- 835 Trumbo, S. K., Brown, M. E., & Hand, K. P. (2019). Sodium chloride on the surface of  
836 europa [Journal Article]. *Science advances*, *5*(6), eaaw7123.
- 837 Vance, S. D., Barge, L. M., Cardoso, S. S., & Cartwright, J. H. (2019). Self-assembling  
838 ice membranes on europa: Brinicle properties, field examples, and possible energetic  
839 systems in icy ocean worlds [Journal Article]. *arXiv preprint arXiv:1903.01584*.
- 840 Vance, S. D., & Brown, J. M. (2013). Thermodynamic properties of aqueous  $\text{MgSO}_4$  to  
841 800 mpa at temperatures from -20 to 100° c and concentrations to 2.5 mol  $\text{kg}^{-1}$  from  
842 sound speeds, with applications to icy world oceans [Journal Article]. *Geochimica et*  
843 *Cosmochimica Acta*, *110*, 176-189.
- 844 Vance, S. D., Hand, K. P., & Pappalardo, R. T. (2016). Geophysical controls of chemical  
845 disequilibria in europa [Journal Article]. *Geophysical Research Letters*, *43*(10), 4871-  
846 4879.
- 847 Vance, S. D., Journaux, B., Hesse, M., & Steinbrügge, G. (2020). The salty secrets  
848 of icy ocean worlds [Journal Article]. *Journal of Geophysical Research: Planets*,  
849 e2020JE006736.
- 850 Waite, J. H., Glein, C. R., Perryman, R. S., Teolis, B. D., Magee, B. A., Miller, G., ...  
851 Bouquet, A. (2017). Cassini finds molecular hydrogen in the enceladus plume: evidence  
852 for hydrothermal processes [Journal Article]. *Science*, *356*(6334), 155-159.
- 853 Wakatsuchi, M., & Saito, T. (1985). On brine drainage channels of young sea ice [Journal  
854 Article]. *Annals of glaciology*, *6*, 200-202.
- 855 Walker, C., Schmidt, B., & Bassis, J. (2014). Breaking the ice: On the application of  
856 fracture system mechanics and fragmentation theory to the chaos regions of europa  
857 [Journal Article]. *LPI(1777)*, 2659.
- 858 Wells, A. J., Hitchen, J. R., & Parkinson, J. R. (2019). Mushy-layer growth and convection,  
859 with application to sea ice [Journal Article]. *Philosophical Transactions of the Royal*  
860 *Society A*, *377*(2146), 20180165.
- 861 Wells, A. J., Wettlaufer, J., & Orszag, S. (2011). Brine fluxes from growing sea ice [Journal  
862 Article]. *Geophysical Research Letters*, *38*(4).
- 863 Wells, A. J., Wettlaufer, J. S., & Orszag, S. A. (2012). Nonlinear mushy-layer convection  
864 with chimneys: stability and optimal solute fluxes [Journal Article]. *arXiv preprint*  
865 *arXiv:1205.0964*.
- 866 Wettlaufer, J., Worster, M. G., & Huppert, H. E. (1997). Natural convection during  
867 solidification of an alloy from above with application to the evolution of sea ice [Journal  
868 Article]. *Journal of fluid mechanics*, *344*, 291-316.
- 869 Worster, M. G. (1991). Natural convection in a mushy layer [Journal Article]. *Journal of*  
870 *fluid mechanics*, *224*, 335-359.
- 871 Worster, M. G. (1997). Convection in mushy layers [Journal Article]. *Annual Review of*  
872 *Fluid Mechanics*, *29*(1), 91-122.
- 873 Worster, M. G., & Rees Jones, D. W. (2015). Sea-ice thermodynamics and brine drainage  
874 [Journal Article]. *Philosophical Transactions of the Royal Society A: Mathematical,*  
875 *Physical and Engineering Sciences*, *373*(2045), 20140166.
- 876 Zolotov, M. Y., & Kargel, J. (2009). *On the chemical composition of europa's icy shell,*  
877 *ocean, and underlying rocks* (Vol. 431) [Book]. University of Arizona Press Tucson,

878  
879  
880  
881  
882  
883  
884

AZ.

- Zolotov, M. Y., & Shock, E. L. (2001). Composition and stability of salts on the surface of Europa and their oceanic origin [Journal Article]. *Journal of Geophysical Research: Planets*, *106*(E12), 32815-32827.
- Zotikov, I. A., Zagorodnov, V. S., & Raikovsky, J. V. (1980). Core drilling through the Ross ice shelf (Antarctica) confirmed basal freezing [Journal Article]. *Science*, *207*(4438), 1463-1465.

# Supporting Information for ”Dynamics of a Solidifying Icy Satellite Shell”

J. J. Buffo<sup>1</sup>, C. R. Meyer<sup>1</sup>, and J. R. G. Parkinson<sup>2</sup>

<sup>1</sup>Thayer School of Engineering, Dartmouth College, Hanover, NH 03755, USA

<sup>2</sup>Atmospheric, Oceanic and Planetary Physics, Department of Physics, Clarendon Laboratory, University of Oxford, Parks Road,

Oxford OX1 3PU, UK

## Contents of this file

1. Text S1 to S4
2. Figures S1 to S6
3. Movies S1 to S2

## Introduction

Below we include four supplementary sections which aim to bolster the conclusions of the main manuscript. Section S1 provides an independent validation of the two-dimensional multiphase reactive transport model (SOFTBALL (Parkinson et al., 2020)) utilized throughout the work via simulations of sea ice growth and explores the impact of variable permeability on the efficiency of impurity entrainment. Section S2 supports the implementation of a linear conductive profile approximation for estimating the ice-ocean interface thermal gradient by comparing simulated and approximated ice shell thermal profiles. Section S3 builds on and supports the work of Section 3.3 of the main manuscript by comparing the brine channel spacing produced under European conditions to those predicted by contemporary models simulating terrestrial ice-ocean/brine environments (Wells

---

et al., 2011; Parkinson, 2019). Section S4 discusses potential limitations of the single domain Darcy velocity approach for investigating the geometry and longevity of brinicles.

### **Text S1 - Model Validation**

To independently validate the two-dimensional reactive transport model of Parkinson et al. (2020) we simulated the physicochemical evolution of sea ice under simplified polar conditions. Model runs were initiated by assuming the domain was entirely filled with seawater (35 ppt) just above its melting temperature (-1.68C), subject to an undercooled atmosphere above (-23.15C) and an ambient ocean below (-1.68C). To ensure the model produces consistent results across a range of spatial scales (important for our upscaling to the Europa environment), we carried out four different runs at varying resolutions, the results of which can be seen in Figure S1. While it is clear that the detailed structure of brine channels within the ice layer are less well resolved when a coarser resolution is employed, the overall bulk salinity profile of the ice is maintained across all resolutions. This can be seen by horizontally averaging the two-dimensional bulk concentration profiles of Figure S1. The results of such an averaging can be seen in Figure S2, which depicts bulk salinity profiles for all four simulated resolutions of Figure S1. There exists only minor variations in bulk salinity, primarily near the ice-ocean interface, where the coarsest resolution simulation struggles to resolve details of the phase change interface between 0.75-0.85 m. Additionally, the simulated bulk salinity profiles qualitatively and quantitatively match empirical measurements of both natural and laboratory grown sea ice (e.g. (Eicken, 1992; Nakawo & Sinha, 1981; Notz et al., 2005)), exhibiting a characteristic ‘c-shape’ salinity profile with amplified salinities near both the upper ice-atmosphere interface and the basal ice-ocean interface as well as bulk salinity values well within the observational range (Eicken, 1992; Nakawo & Sinha, 1981; Notz et al., 2005). The ability of the model to reproduce bulk salinity profiles of sea ice provides an additional and

independent validation of the model, expanding upon the existing literature (Parkinson, 2019; Parkinson et al., 2020; Wells et al., 2019), and lending confidence to the model's application to planetary ice-ocean systems.

An important, yet under constrained, component of nearly all multiphase ice models is the implementation of a permeability-porosity relationship (e.g. (Golden et al., 2007; Katz & Worster, 2008; Buffo et al., 2020; Parkinson et al., 2020)). This relationship governs the ability of fluid to flow throughout the system and aims to broadly capture the fine-scale microstructural properties of the complex porous ice matrix. This is a common challenge in porous media studies and a range of permeability-porosity relationships exist (Bear, 2013). Our selection of a Kozeny-Carman permeability-porosity relationship for our Hele-Shaw cell simulations is consistent with previous studies of unidirectional ice-brine solidification investigations (Katz & Worster, 2008; Parkinson et al., 2020; Wells et al., 2019). Nevertheless, this relationship (Equation 7 of the main text) relies on the selection of a permeability factor,  $K_0$ . This is akin to the reference permeabilities in the power law permeability-porosity relationships of other multiphase ice-brine system studies (e.g. (Hammond et al., 2018; Golden et al., 2007)). Regardless, the selection of this parameter will impact the permeability, and thus fluid transport, of the system and should reproduce empirical observations of ocean-derived ices. To demonstrate the importance of the permeability factor ( $K_0$ ) we simulated the physicochemical evolution of sea ice (as described above) using a range of permeability factors and compared their resulting bulk salinity profiles. The results of these simulations can be seen in Figure S3. In varying the permeability factor by a factor of 20 bulk salinity in regions of the ice varied by as much as 30%. Such variations can have drastic effects on the properties of the resultant ice, and highlights the need to further constrain our understanding of ocean-derived ice permeability via both experimental and numerical techniques. Our selected value of

$K_0$  used throughout the study  $K_0 = 2 \times 10^{-9} \text{ m}^2$  produces bulk salinity profiles consistent with observations of natural and laboratory grown sea ice (Eicken, 1992; Nakawo & Sinha, 1981; Notz et al., 2005). Furthermore, the Hele-Shaw cell limited Kozeny-Carman relationship employed in our work is consistent with empirically derived power law permeability-porosity relationships for sea ice (Golden et al., 2007). Figure S4 shows a comparison of the power law permeability-porosity relationship derived empirically by Golden et al. (2007), the power law relationship employed in the modeling investigation of Buffo et al. (2020), the Kozeny-Carman permeability-porosity relationship employed in the manuscript (without Hele-Shaw cell limitation), and the same Kozeny-Carman permeability-porosity relationship when it is employed in a Hele-Shaw cell, limiting the permeability of the free fluid to a finite value. While there are slight variations in the predicted permeability values, for porosities relevant to the interior of the mushy layer ( $\phi < 0.8$ ) predicted permeabilities are within two orders of magnitude.

### **Text S2 - Ice Shell Thermal Profile**

To demonstrate the validity of implementing the simple linear conduction approximation for the ice-ocean interface thermal gradient (Equation 8 of the main text), we compare the thermal profile during a selected simulation to that predicted by the linear conduction approximation:

$$T(z) = T_s + \frac{T_{oc} - T_s}{H_{shell}} z \quad (1)$$

where  $z$  is depth beneath the surface,  $T_{oc}$  is ocean temperature,  $T_s$  is the surface temperature, and  $H_{shell}$  is the thickness of the ice shell. The results of this comparison can be seen in Figure S5. The profiles vary only slightly, with true temperatures being slightly higher throughout the majority of the shell. This is an expected result as the ice-ocean interface mushy layer will buffer heat loss to the cold upper surface due to the lower ther-

mal conductivity of brine compared to ice. Such variations in ice shell thermal profiles have previously been shown to have a negligible affect on interface dynamics and ice shell physicochemical characteristics (Buffo et al., 2020).

### **Text S3 - Brine Channel Spacing**

The distribution of brine channels in the mushy layer plays a fundamental role in the desalination and structure of the ice-ocean interface, and thus the physicochemical properties of ocean-derived ices. Channel spacing is a dynamic property and depends on a number of environmental pressures which control convective motion in the porous region near the ice-ocean phase boundary. Brine channel spacing in saltwater systems has previously been investigated, both experimentally (Wakatsuchi & Saito, 1985; Tison & Verbeke, 2001) and theoretically (Wells et al., 2011; Parkinson, 2019). Wells et al. (2011) and Parkinson (2019) demonstrate that the non-dimensional brine channel aspect ratio, defined as:

$$a_s = \frac{L}{2h} \quad (2)$$

where  $L$  is the horizontal distance between brine channels and  $h$  is the thickness of the ice-ocean interface mushy layer, is strongly controlled by the mush Rayleigh number (Wells et al., 2011; Parkinson, 2019):

$$Ra_{ML} = \frac{K_0 \rho_{br} g \beta \Delta C h}{\kappa_{br} \eta} \quad (3)$$

where  $K_0$  is a characteristic permeability,  $\rho_{br}$  is the density of the underlying ocean/brine,  $g$  is gravity,  $\beta$  is the solutal contraction coefficient,  $\Delta C$  is the difference in salinity between the eutectic concentration and the underlying fluid,  $h$  is mushy layer thickness,  $\kappa_{br}$  is the thermal diffusivity of the underlying fluid, and  $\eta$  is dynamic fluid viscosity.

To investigate the relationship between ice-ocean interface environment and brine channel spacing, in both planetary and terrestrial systems, we measured brine channel aspect ratios for seven simulations (ice shell depths ranging from 10 m to 1000 m) under European conditions and compare our results to those of Wells et al. (2011) and Parkinson (2019) (Figure S6). Additionally, we measured brine channel aspect ratios during a simulation of sea ice to ensure our results agree with those of Parkinson (2019) who simulate the top-down solidification of sea ice under a range of thermal forcing and during a simulation where a concentration ratio  $\mathcal{C}=1$  is implemented to bridge the existing gap between the concentration ratios investigated by Wells et al. (2011) ( $\mathcal{C}=2,5,10,15$ ) and those utilized in Parkinson (2019) and the current work ( $\mathcal{C}=0.18$ ). Following Wells et al. (2011), the concentration ratio is defined as:

$$\mathcal{C} = \frac{C_0 - C_s}{C_e - C_0} \quad (4)$$

where  $C_0$  is the salinity of the underlying fluid,  $C_s$  is the salinity of ice (here taken to be zero), and  $C_e$  is the eutectic concentration.

Our simulation results, as well as the results of Wells et al. (2011) and Parkinson (2019), show a general trend of decreasing brine channel aspect ratio with increasing mush Rayleigh number, approaching a steady state value for  $Ra_{ML} \gg Ra_c$ , as reported by Wells et al. (2011), where  $Ra_c$  is the critical Rayleigh number where mushy layer convection initiates. This suggests that after onset of convection in the mushy layer the rate of mushy layer thickening (increasing  $h$ ) outpaces the collapse/merging of brine channels (a phenomenon well documented in the literature by both experimental and modeling studies, which leads to increasing  $L$ ), until a steady state aspect ratio is achieved. The primary environmental factor affecting the value of the steady state aspect ratio is the concentration ratio, for while simulations of sea ice and European ice had substantially

different environmental forcing (gravity, characteristic permeability) their steady state aspect ratios vary minimally when compared to the difference in steady state aspect ratios of simulations with variable concentration ratios. An additional control on brine channel spacing is the finite width of our simulation domain, which necessarily quantizes the number of brine channels. We have taken care to select domain widths which facilitate a large number of brine channels whenever possible to reduce the impact of this numerical limitation. Another interesting feature of the simulations presented in Figure S6 is the existence of convective modes; apparent in all simulations except those of Wells et al. (2011), due to their method of selecting  $L$  such that it maximized solute flux from the mushy layer (Wells et al., 2012) and observing the evolution of  $h$ , as jumps between well defined groupings that are well represented by the inverse fits of Figure S6 (additionally, transition between convective modes can be seen in Supplementary Movie S1 and S2 as brine channels collapse and reform). This alternation between quasi-stable convective modes in a confined porous media is a well documented natural phenomenon (e.g. (Karani & Huber, 2017)) which we believe is amplified by the finite resolution of the simulations. That is, as the resolution is coarsened, as is needed to simulate thicker mushy layers deep within the ice shell of Europa, the lower modes (associated with smaller aspect ratios) are likely not explicitly resolved by the simulation. This does not affect the accuracy of the physicochemical results of the model, however, as it was shown in Section S1 that bulk salinity profiles remain constant regardless of whether discrete brine channels are resolved (e.g. Figures S1–S2).

Due to the rapid rate at which ice-ocean systems exceed their critical Rayleigh numbers (e.g. the presence of brine channels in thin sea ice (Wettlaufer et al., 1997; Cox & Weeks, 1974)) we conclude that the thick ice shells of icy worlds such as Europa should have ice-ocean interfaces characterized by brine channel aspect ratios near their steady

state limit. This suggests progressively widening channel spacing as the ice shell thickens that will scale with mushy layer thickness. Given the results of Section 3.2 of the main manuscript (that mushy layer thickness can be well approximated as a linear function of ice shell thickness, linear relationship coefficient=0.0539), and noting that the steady state brine channel aspect ratio is 0.08 (Blue lines of Figure S6), European ice shells of thickness 1 km, 10 km, and 30 km would have expected brine channel spacing of 8.62 m, 86.2 m, and 259 m, respectively. Constraining channel spacing is important in understanding the desalination and heterogeneity of the lower ice shell, which may have substantial implications for the geophysical processes and habitability of ice-ocean worlds, as outlined in the main manuscript.

#### **Text S4 - A Note on Simulated Brinicle Geometry**

It is important to note that the geometry of the brinicles simulated in Section 3.3 may be impacted by the Darcy approximation implemented in the SOFTBALL code. The Darcy technique is employed to simplify the ice-ocean system and involves simulating the entire domain (liquid and solid) as a porous media (rather than solving Darcy's law in the porous region and the Navier-Stokes equation in the fluid). This is a widely used method and its accuracy hinges on the large amplification of permeability in the fluid region (compared to the porous region). A large, but finite, permeability means flow is faster in the fluid than in the porous region (ensuring accurate evolution of the multiphase layer), while still being computationally tractable and avoiding a difficult boundary value problem. The reduction of flow speed in the free fluid from its true value (permeability  $\neq$  infinity), however, means that diffusive processes are likely overly expressed in the fluid region. This could lead to amplified spacing between brinicle walls beneath downwelling high salinity regions (e.g. Figure 6). In the real system downwelling plumes will not be subject to a finite permeability and are likely to be more jet-like, reducing dissipative

flow near the interface and potentially supporting more stable, longer-lived ice structures than suggested in Section 3.3 (See Wells et al. (2019)). We therefore suggest our results be taken as a lower limit for the longevity of brinicle structures at Europa's ice-ocean interface.

### Movie S1.

Nondimensional bulk salinity evolution under European conditions. (Domain: 20m x 20m (512 x 512 grid), Resolution: 3.9cm)

### Movie S2.

Porosity evolution under European conditions. (Domain: 20m x 20m (512 x 512 grid), Resolution: 3.9cm)

## References

- Bear, J. (2013). *Dynamics of fluids in porous media* [Book]. Courier Corporation.
- Buffo, J. J., Schmidt, B. E., Huber, C., & Walker, C. C. (2020). Entrainment and dynamics of ocean-derived impurities within europa's ice shell [Journal Article]. *JGR: Planets*.
- Cox, G. F. N., & Weeks, W. F. (1974). Salinity variations in sea ice [Journal Article]. *Journal of Glaciology*, 13(67), 109-120.
- Eicken, H. (1992). Salinity profiles of antarctic sea ice: field data and model results [Journal Article]. *Journal of Geophysical Research: Oceans*, 97(C10), 15545-15557.
- Golden, K. M., Eicken, H., Heaton, A. L., Miner, J., Pringle, D. J., & Zhu, J. (2007). Thermal evolution of permeability and microstructure in sea ice [Journal Article]. *Geophysical Research Letters*, 34(16).
- Hammond, N. P., Parmentier, E., & Barr, A. C. (2018). Compaction and melt transport in ammonia-rich ice shells: Implications for the evolution of triton [Journal Article]. *Journal of Geophysical Research: Planets*, 123(12), 3105-3118.

- Karani, H., & Huber, C. (2017). Transitional behaviour of convective patterns in free convection in porous media [Journal Article]. *Journal of Fluid Mechanics*, 818.
- Katz, R. F., & Worster, M. G. (2008). Simulation of directional solidification, thermochemical convection, and chimney formation in a hele-shaw cell [Journal Article]. *Journal of Computational Physics*, 227(23), 9823-9840.
- Nakawo, M., & Sinha, N. K. (1981). Growth rate and salinity profile of first-year sea ice in the high arctic [Journal Article]. *Journal of Glaciology*, 27(96), 315-330.
- Notz, D., Wettlaufer, J. S., & Worster, M. G. (2005). A non-destructive method for measuring the salinity and solid fraction of growing sea ice in situ [Journal Article]. *Journal of Glaciology*, 51(172), 159-166.
- Parkinson, J. R. G. (2019). *Nonlinear convection in sea ice and other mushy layers* (Thesis). University of Oxford.
- Parkinson, J. R. G., Martin, D. F., Wells, A. J., & Katz, R. F. (2020). Modelling binary alloy solidification with adaptive mesh refinement [Journal Article]. *Journal of Computational Physics: X*, 5, 100043.
- Tison, J.-L., & Verbeke, V. (2001). Chlorinity/salinity distribution patterns in experimental granular sea ice [Journal Article]. *Annals of Glaciology*, 33, 13-20.
- Wakatsuchi, M., & Saito, T. (1985). On brine drainage channels of young sea ice [Journal Article]. *Annals of glaciology*, 6, 200-202.
- Wells, A. J., Hitchen, J. R., & Parkinson, J. R. (2019). Mushy-layer growth and convection, with application to sea ice [Journal Article]. *Philosophical Transactions of the Royal Society A*, 377(2146), 20180165.
- Wells, A. J., Wettlaufer, J., & Orszag, S. (2011). Brine fluxes from growing sea ice [Journal Article]. *Geophysical Research Letters*, 38(4).
- Wells, A. J., Wettlaufer, J. S., & Orszag, S. A. (2012). Nonlinear mushy-layer convection

with chimneys: stability and optimal solute fluxes [Journal Article]. *arXiv preprint arXiv:1205.0964*.

Wettlaufer, J., Worster, M. G., & Huppert, H. E. (1997). Natural convection during solidification of an alloy from above with application to the evolution of sea ice [Journal Article]. *Journal of fluid mechanics*, *344*, 291-316.

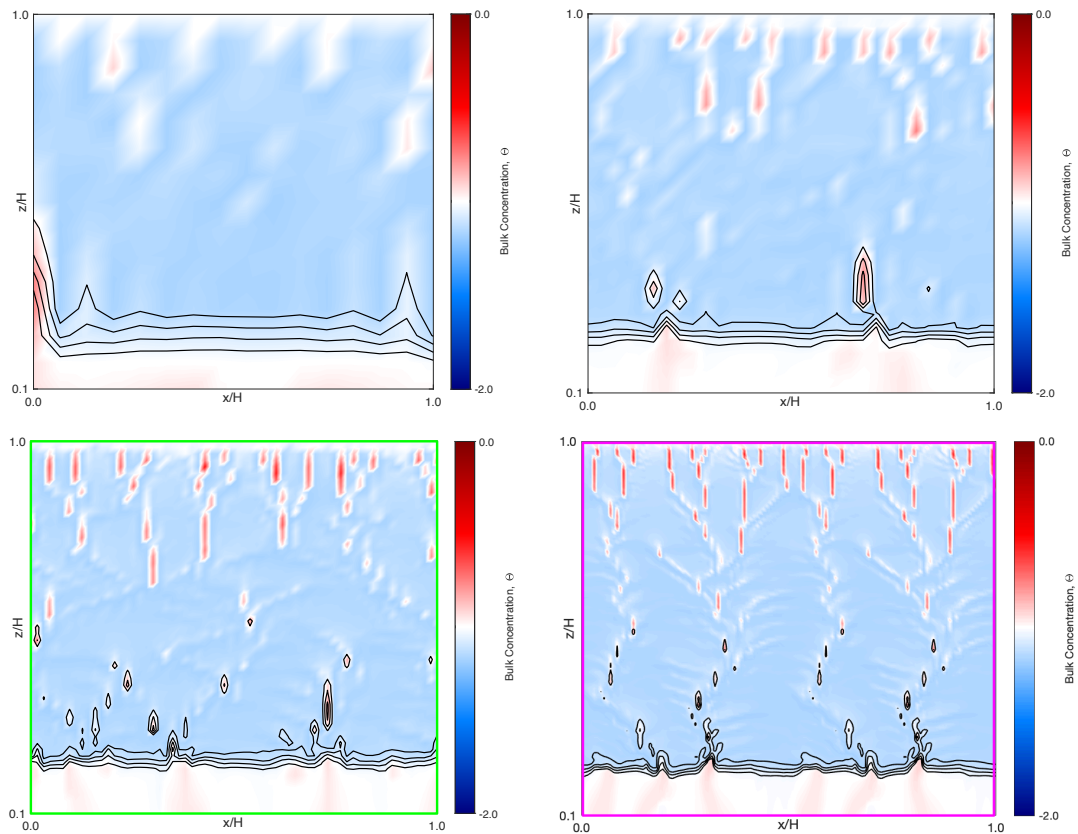


**Figure S1.** The effects of variable resolution. **Top Left)** 16x16 starting grid, no Adaptive Mesh Refinement (AMR) (6.25 cm resolution). **Top Right)** 32x32 starting grid, no AMR (3.13 cm resolution). **Bottom Left)** 32x32 starting grid, 1 level AMR (1.56 cm resolution). **Bottom Right)** 32x32 starting grid, 2 level AMR (0.78 cm resolution).

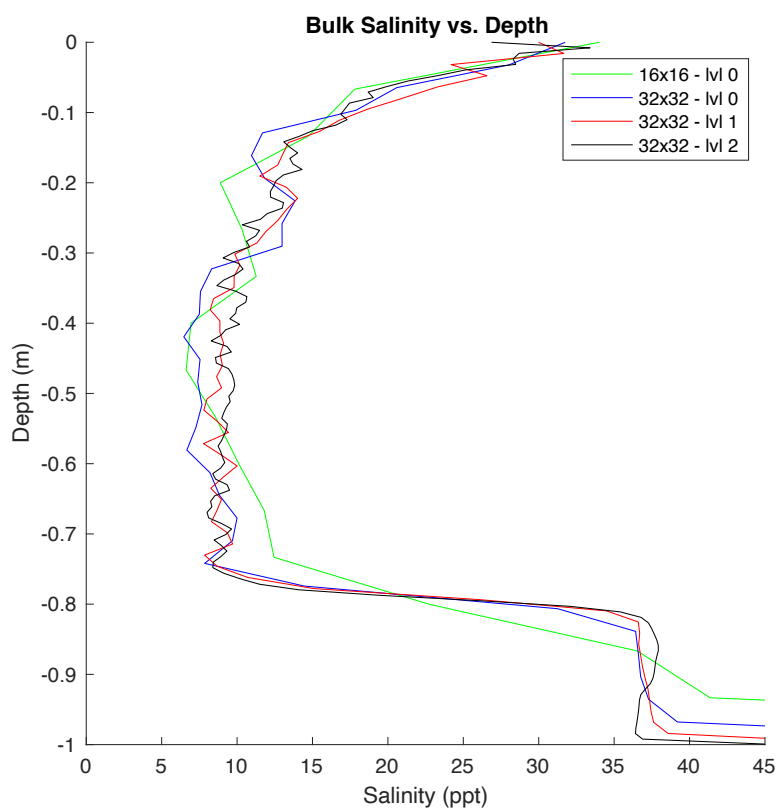


**Figure S2.** Horizontally averaged bulk salinity profiles. Using the results of Figure S1, bulk salinity is horizontally averaged and compared. Profiles have characteristic ‘c-shape’ of first year sea ice, with appropriate bulk salinity values, and are in good agreement across all resolutions.

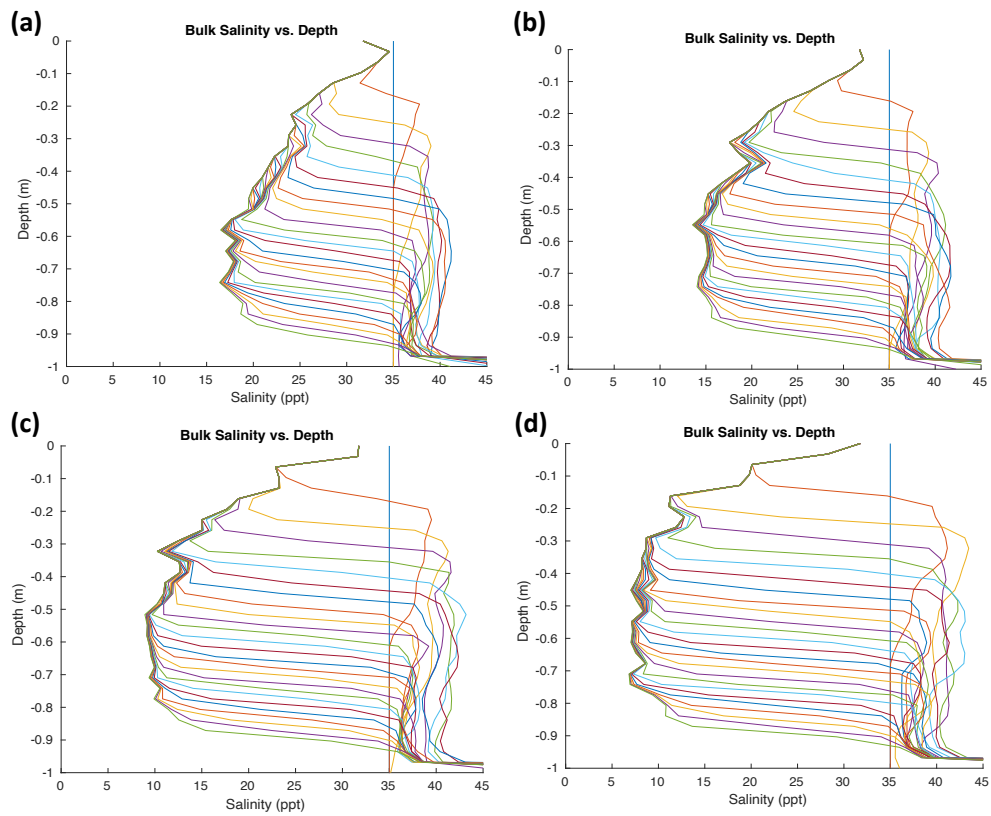


**Figure S3.** The effects of variable permeability factors on sea ice bulk salinity. Horizontally averaged bulk salinity profiles of sea ice generated using identical conditions less the permeability factor,  $K_0$ . **a)**  $K_0 = 1e^{-10}$ . **b)**  $K_0 = 2e^{-10}$ . **c)**  $K_0 = 8e^{-10}$ . **d)**  $K_0 = 2e^{-9}$ . In all plots colors represent progressive temporal snapshots during the simulation (as the ice thickens).

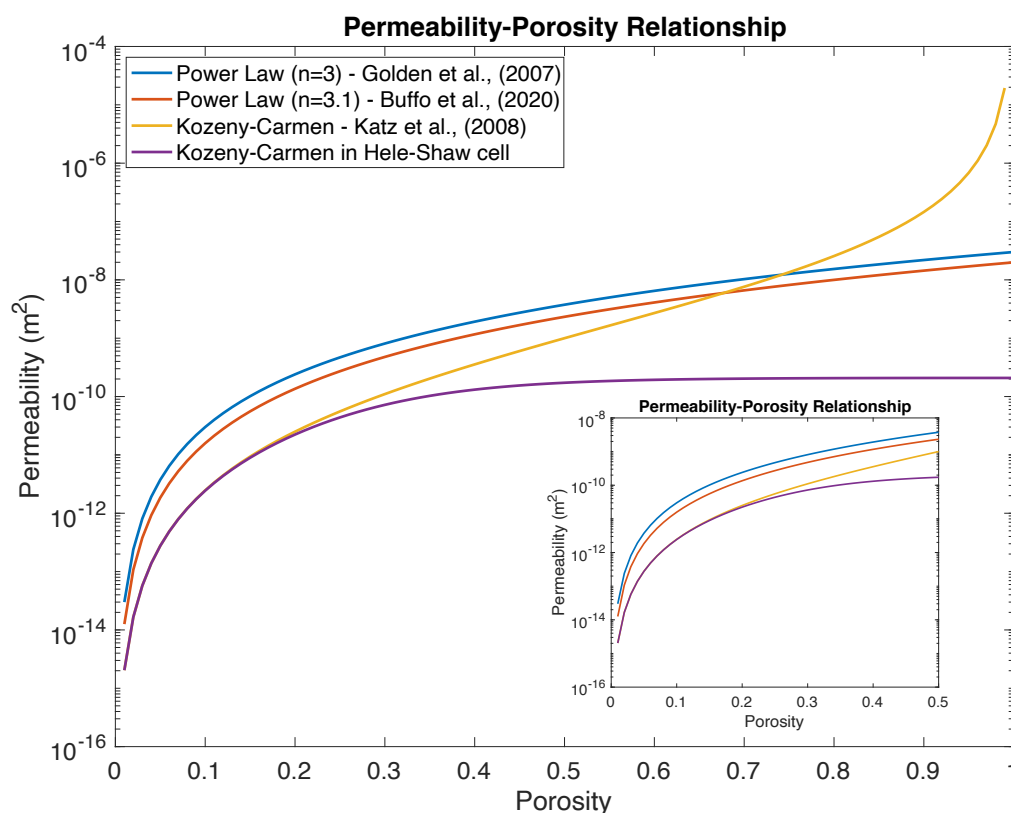


**Figure S4.** A comparison of common permeability-porosity relationships. The modified Kozeny-Carmen relationship of Parkinson et al. (2020) (purple line), employed here, is comparable to the Kozeny-Carmen relationship of Katz and Worster (2008) as well as the power law relationships of Golden et al. (2007) and Buffo et al. (2020). The Hele-Shaw cell modifications place a finite limit on the permeability of the underlying fluid ( $\phi \rightarrow 1$ ).

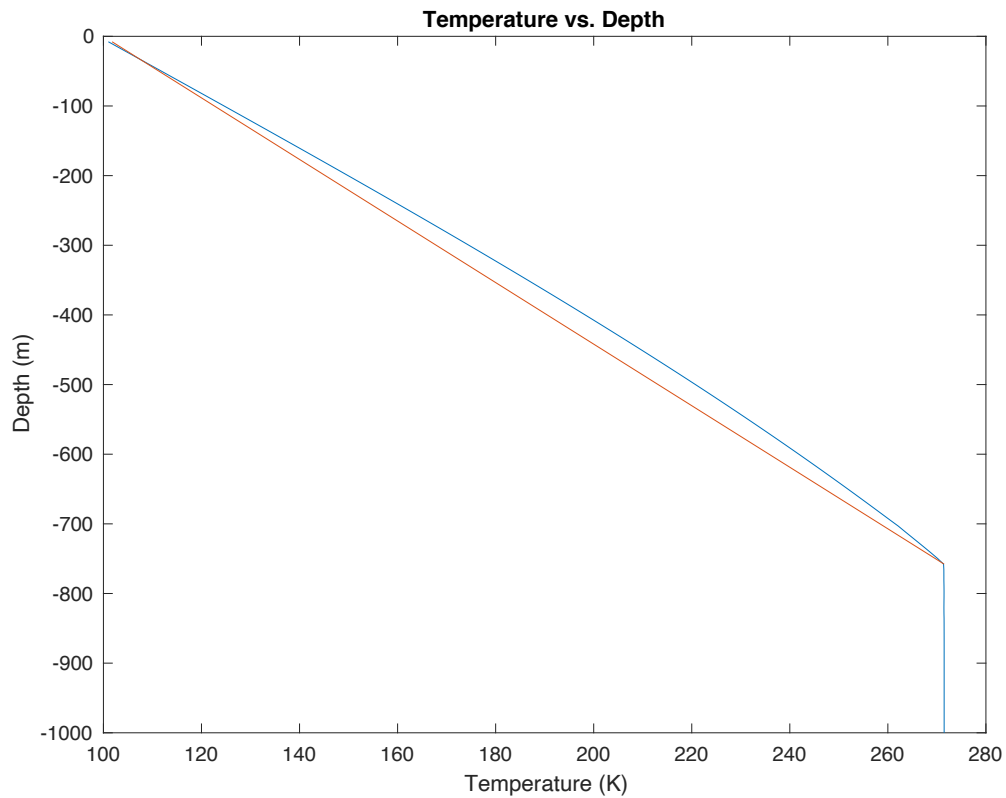


**Figure S5.** Thermal profiles in an ice shell. The blue curve is the horizontally averaged temperature profile extracted from a top-down solidification simulation under Europa conditions. The ice-ocean interface occurs at  $\sim 758$  m below the surface. The red curve is the linear conduction approximation given by Equation S1.

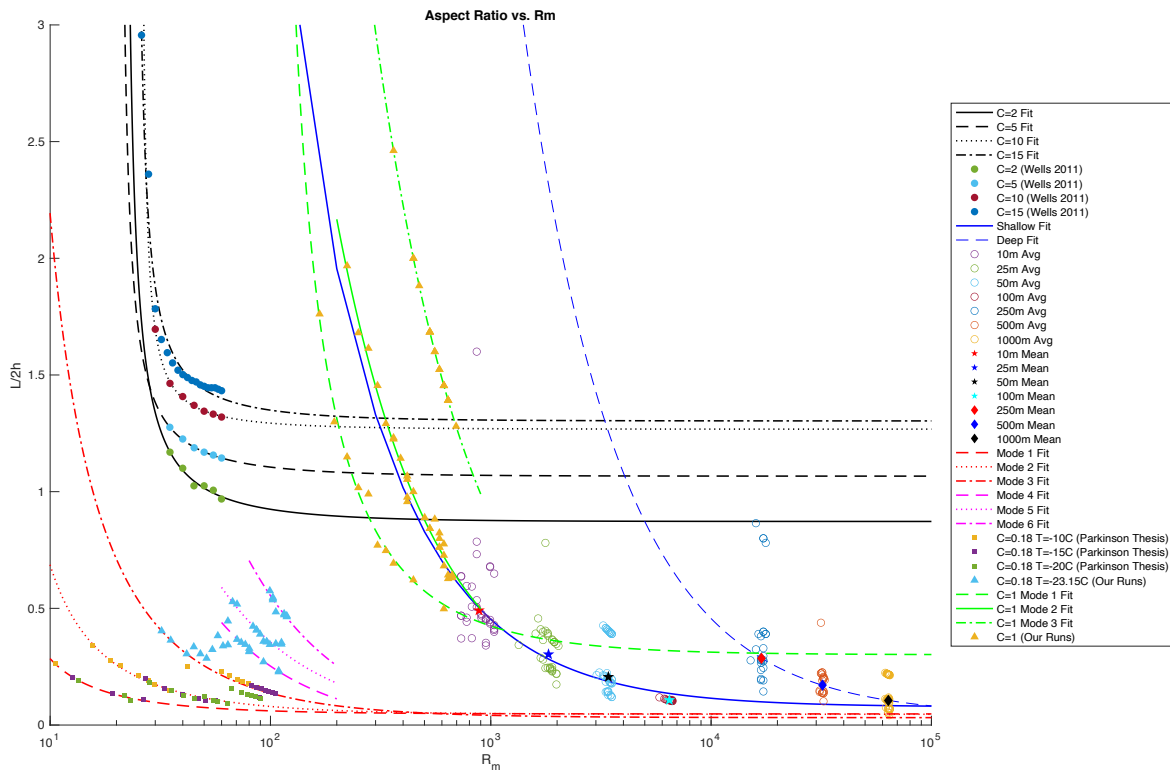


**Figure S6.** Brine channel aspect ratio as a function of mush Rayleigh number. Solid circles are results from Wells et al. (2011) and black curves are inverse fits to this data. Solid squares are results from Parkinson (2019) (Chapter 5.1.5) and red curves are inverse fits to this data. Open circles and solid stars/diamonds are simulation results and mean values for European environments runs, respectively, and blue curves are inverse fits to this data. Blue and yellow solid triangles correspond to our sea ice and  $\mathcal{C} = 1$  simulations, respectively, and the pink and green curves are their associated inverse fits. As the mush Rayleigh number increases brine channel aspect ratios approach a steady state value primarily governed by the concentration ratio, in agreement with the results of (Wells et al., 2011). ‘Modes’, as listed in the figure legend, are associated with mushy layer convective modes within simulation domains. These quasi-steady states are a common feature of convection in a confined porous media (Karani & Huber, 2017) and are amplified by the finite resolution of simulations.